STRENGTH CHARACTERISTICS OF THE HORSESHOE VORTEX

A Thesis Submitted
in Partial fulfilment of the Requirements
for the Degree of
MASTER OF TECHNOLOGY

by

PRABHA SHRIVASTAVA

to the

DEPARTMENT OF CIVIL ENGINEERING
INDIAN INSTITUTE OF TECHNOLOGY, KANPUR

JANUARY, 1989

CE-1989-M-SHR-STR

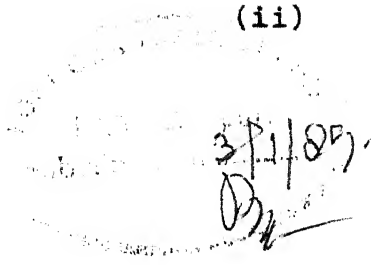

CERTIFICATE

The thesis entitled 'STRENGTH CHARACTERISTICS OF HORSE SHOE VORTEX' by Prabha Shrivastava (Roll No.8620325) is hereby approved as a creditable report on research carried out and present in a manner which warrants its acceptance as a prerequisite for the degree of Master of Technology. The work has been carried out under my supervision and has not been submitted elsewhere for a degree.

January , 1989

(Dr. T. GANGADHARAIAH)
Professor
Department of Civil Engineering
Indian Institute of Technology, Kanpur

CONTENTS

LIST OF FIGURES

LIST OF TABLES

LIST OF NOTATIONS

b	width of the rectangular pier
x_c	distance of the vortex centre from the pier
y_c	distance of the vortex centre from the wall plate
x_s	distance of the separation line from the pier
h_c	height of the centre line of the blower opening from the wall plate
D_o	vertical dimension of the vortex
P_e	perimeter of the velocity contour
V_θ	rotational velocity
ω	vorticity
ω_c	vorticity per circular vortex
δ	boundary layer thickness
δ_*	displacement boundary layer thickness
U_m	maximum velocity of flow at the position of pier in the absence of pier
$\bar{U}$	average velocity of undisturbed flow
Re_b	Pier Reynolds number based on pier width
$V_{.\theta}$	strength of horse shoe vortex computed from velocity contours
$\Gamma_{c_{p\omega}}$	strength of horse shoe vortex computed from pressure coefficient curve on wall
$\Gamma_{c_{pc}}$	strength of horse shoe vortex computed from the pressure coefficient curve at the level of vortex centre
c_p	pressure coefficient
Δc_p	difference in pressure coefficients between crests and troughs of pressure distribution
U_*	shear velocity (m/s)
ν	kinematic viscosity of air

ρ_a	mass density of air
$2r$	width of the crest of the pressure distribution

ABSTRACT

The present investigation has laid stress on the computation of the strength of the horseshoe vortex formed upstream of the rectangular pier mounted on the rigid wall. On the basis of detailed measurement of velocity and static pressure on the line of symmetry in the separating zone, strength of the vortex has been computed separately from velocity and pressure distributions. The magnitude of the vortex strength computed from the velocity distribution and the pressure distribution on the wall are found to be nearly same. A relationship has been established between the strength computed from pressure distributions on the wall and at the level of the centre of the vortex, and it is found that the latter is twice that of the former value. The strength and some other characteristics of the horseshoe vortex like location of the vortex, rotational velocity, angular velocity and size have been computed from the present data and compared with the results of previous investigators.

CHAPTER - 1

INTRODUCTION AND LITERATURE SURVEY

1.1 Introduction:

Presence of any obstruction to the flow of fluid gives rise to adverse pressure gradient. In the region of adverse pressure gradient, the leading edge of the obstruction serves as a device for concentrating the vorticity present in the approaching flow, and forms a vortex system due to a three dimensional separation of boundary layer. The lower regions of the separated boundary layer roll up to form the vortex system upstream of the obstruction such as bridge pier. This vortex system assumes a characteristic shape of horse-shoe and this has led to its name - horse shoe vortex. Such vortex system is known to form around the bridge pier set in the river bed, tall building junction with ground etc. It has been observed that this flow structure in the form of horse-shoe vortex develops irrespective of whether the bed is rigid or mobile. In case of mobile bed, the horse shoe vortex system plays an active role in local scour around the bridge pier set in river bed.

The dominant feature of the scour process around pier is the horse shoe vortex system. If the strength of this system is strong enough to overcome the particle's resistance to motion, scour will be initiated. Sediment particles will be dislodged from upstream of the pier and carried out of the scour hole by the horse shoe vortex system and/or by wake vortex system in the down stream side of the pier. Magnitude of the scour depth depends on the strength of the horse-shoe

vortex along with the other flow and geometry parameters.

From the physical mechanism and theoretical understanding point of view, the earlier investigations in the horse-shoe vortex flows appear to have been made by Squire and Winter (1951), Howthrone (1954) and Taylor (1967), as part of their studies on secondary flows in turbomachines (A.K. Gupta and T. Gangadharaiah, 1988). Shen, Scheneider and Karaki (1969) emphasised the importance of pier geometry and Reynolds number on the local scour. Similarity parameters characterising the horse shoe vortex flows were investigated experimentally by Belik (1973) in a low speed wind tunnel with approaching boundary layers both laminar and turbulent. Baker (1979, 1980a, 1980b) made extensive measurements of static pressure in the separated region of laminar and turbulent horse shoe vortices and showed the importance of Reynolds number for laminar horse shoe vortex. Using a fixed bed model of local scour zone, Melville and Raudkivi (1977) measured the turbulence intensities and the boundary shear stresses. Depending on the Reynolds number and bed conditions the scour zone may contain more than one vortices. But it is the primary horse shoe vortex which controls the local scour depth. Therefore, attempts have been made to estimate the vortex strength, core diameter and the vortex centre location of the primary horse shoe vortex.

Baker's measurements (1979, 1980a) put the vortex centre location at about 0.2-0.3 diameter upstream of the cylinder leading edge. The core diameter is found to be about one half the cylinder diameter in the beginning of the

Hawthrone (1954), (Belik 1973) carried out an analysis of the induced vorticity and its effects in shear flow with respect to the non-uniform distribution of inlet velocity moving past cylindrical bodies.

Shen et al. (1969) concluded from the analysis of the flow field and the horse shoe vortex system near the circular pier that the circulation of the vortex is proportional to pier Reynold's number.

Belik (1973) visualized the vortex flow pattern in non-uniform flow near the junction between a circular cylinder and flat plate in a low speed wind tunnel. He measured the pressure distribution on the line of symmetry on the bed at the junction of circular cylinder and showed a depression in the pressure distribution associated with the presence of horse-shoe vortex. The experiment of Belik, related the separation region with the Reynolds number based on boundary layer thickness.

Five types of vortex regimes depending upon the velocity of flow were mentioned by Schwind in 1962 (Baker, 1979). The flow passed from 'regime 1' to 'regime 5' as the velocity increases (Fig.1.1). At the lower velocities, no vortices were visible. Steady clockwise rotating vortices and counter rotating vortices were observed at increased velocities. The number of vortices was found to increase with the increase in velocity. At higher velocities, for 'regime 4', the primary vortex was seen to combine with the secondary vortex, and for 'regime 5',the vortex presumably combined

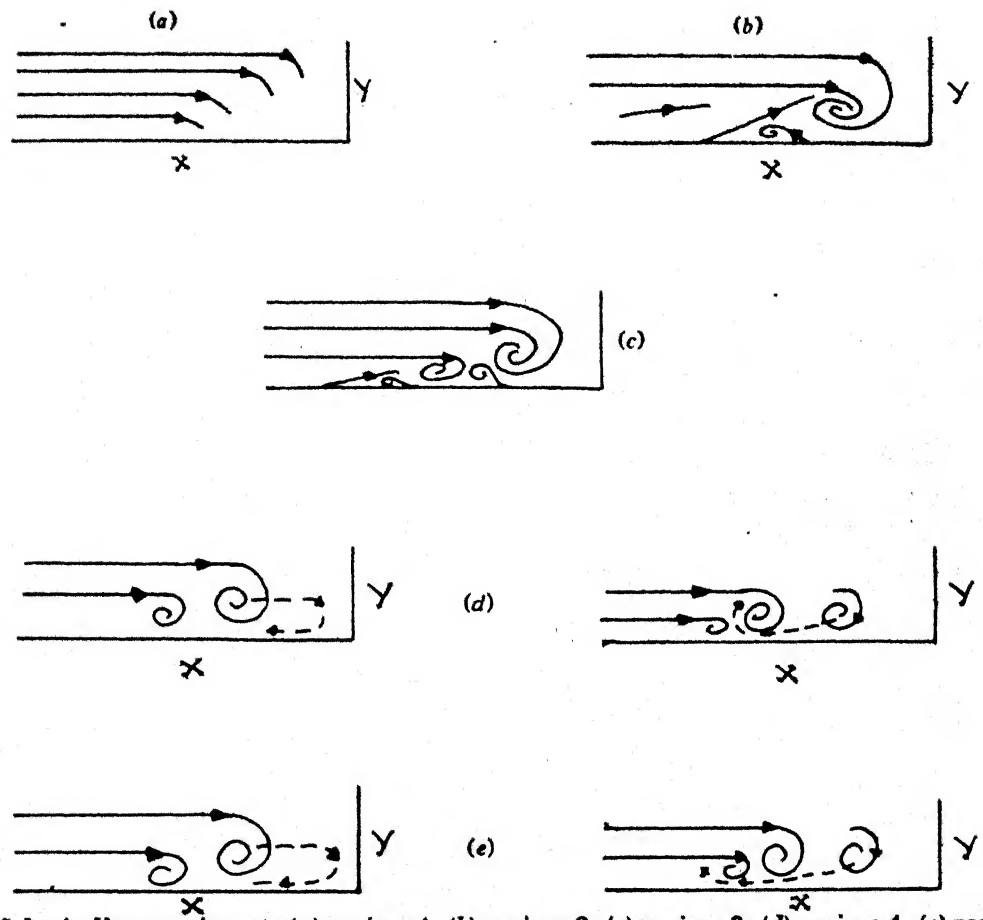

Fig.1.1 Schwind's experiment: (*a*) regime 1; (*b*) regime 2; (*c*) regime 3; (*d*) regime 4; (*e*) regime 5. (Baker . . 197

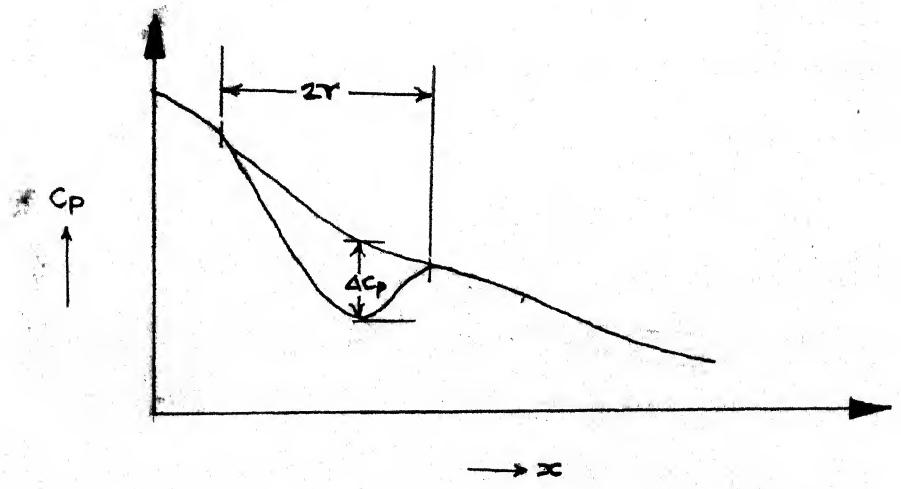

Fig. 1.2 : Illustration of C_p Curves

with an unobserved third clockwise rotating vortex. However, a well defined demarcation of different regimes was not possible.

Baker (1979) investigated the horse shoe vortex formed around the base of a circular cylinder by a separating laminar boundary layer. He measured the pressure distributions beneath the vortex system and determined the variation of horse-shoe vortex position on the plane of symmetry upstream of the cylinder. Smoke flow visualization showed that the dips in pressure distributions correspond to the centre of the primary horse-shoe vortex. The vortex systems were observed with 2, 4 and 6 vortices, the number of vortices increasing as pier Reynolds number $\frac{VD}{\nu}$ increases. Baker related the position of primary horse-shoe vortex to pier Reynold's number $(\frac{VD}{\nu})$ and D/δ^*, where D is pier diameter, δ^* is displacement thickness, V is maximum velocity of flow, ν is kinematic viscosity of flow. The non-dimensionalized vortex position was found to increase as $\frac{VD}{\nu}$ increases and D/δ^* decreases. Flow velocity measurements were made within the vortex systems. The radial flow component measured in two vortices was found to increase linearly with the distance from the centre of the vortex in the central region of the vortex. Skin friction coefficient was also measured beneath the primary vortex.

Measurements of Baker (1980) are concerned with flow parameters for the turbulent horse shoe vortex. His experiments revealed how the primary and secondary separation lines varied with the flow parameters. The non-dimensionalized

vortex position $x_{V/D}$ was found to be a function of pier Reynolds number $\frac{VD}{\nu}$ and D/δ^* as in case of laminar horse shoe vortex. The positions of both primary and secondary separation lines appeared to vary with D/δ^* and Reynolds number based on displacement thickness $\frac{U\delta_*}{\nu}$.

Qadar (1981) measured the velocity distribution in the vertical in the core of turbulent horse shoe vortex in open channel flow. He showed that the size of the horse shoe vortex remains constant at approximately 0.2 times the pier width, and that its velocity is a function of the average velocity of flow.

Baker (1985) presented formulae for the positions of the point of zero shear stress (at the separation position) and the point of maximum shear stress (beneath the main vortex) upstream of the circular cylinder mounted normal to flat plate. These positions were related to various parameters, viz, boundary layer displacement thickness Reynolds number $V\delta^*/\nu$, the ratio of boundary layer displacement thickness to cylinder diameter, and the ratio of cylinder height to cylinder diameter.

In wind tunnel, Gupta (1984) measured the pressure distribution on the plate and circular cylinder, located the vortex zone and developed a method to compute the strength of the horse-shoe vortex. He observed the presence of three major vortices on the plate in the front of the cylinder. The separation point on the plate upstream of the cylinder has been found to occur around $\frac{x}{D} = 1.0$, where x is the distance measured from the front nose and D is the diameter of the circular cylinder. He postulated that the strength of primary

vortex must be proportional to the pressure difference between the crest and trough of the pressure distribution

$$\Gamma_{c_p}^{*} = \frac{\Gamma_{c_p}}{\pi D\, U_m} = \frac{2r}{D}\sqrt{\Delta C_p}$$

where 2 r is the width of the crest of the pressure distribution as shown in Fig. 1.2.

Muzzammil (1985) computed the strength of the horse shoe vortex from the pressure distribution in the separating region at the base in open channel. He related the vortex strength to the flow parameter defined as $\frac{U_o D}{U_* \delta}$, where U_o is the maximum velocity of flow, U_* is the shear velocity D is the diameter of the cylinder and δ is the boundary layer thickness.

Gangadharaiah, Muzzammil, and Subramanya (1986) measured the pressure distribution in the separating zone at the base of the plate. The initial vortex strength from pressure distribution and equilibrium vortex strength from the threshold velocity were estimated. The relationship of these strengths were used to obtain an expression for the equilibrium scour depth.

Muzzammil et al. (1989) investigated the vorticity characteristics of scouring horse-shoe vortex around a bridge pier. The size, strength, and vorticity of the horse-shoe vortex before the scour were computed from pressure distribution and velocity profiles in the separating region at the base plate of the cylinder.

1.3 Present Investigation:

Detailed flow structure near the junction of pier and wall like velocity, direction of flow and pressure distribution on the line of symmetry in the separating region has not been reported in literature. However, the velocity profile at the centre of the vortices and pressure distribution on the surface of the pier model and on the wall plate have been obtained by various investigators mentioned earlier.

In the present investigation an attempt has been made to measure the magnitude and direction of velocity, and static pressure distribution on the line of symmetry. Based on this data the strength of the horse shoe vortex computed separately from velocity distribution and from pressure distribution in the vortex zone are related with each other. The horse shoe vortex characteristics like strength, rotational velocity, angular velocity and size are related with Reynolds number based on pier width.

CHAPTER - 2

EXPERIMENTS AND METHODOLOGY

2.1 General:

In the present study, the characteristics of the horse shoe vortex formed in front of the rectangular pier plate have been studied. Pressure distribution on the line of symmetry on wall and on rectangular plate are measured.

Velocity measurements have been made in vertical sections upstream of the plate using a Keal probe. Static pressure distribution has been measured using wedge probe. Vorticity has been measured using the vorticity probe. The strength of horse shoe vortex has been computed using velocity distribution and pressure distribution separately.

2.2 Experimental Set-up:

The schematic of the experimental set up is shown in Fig.(2.1). A rectangular plate of 5 cm.width, 40 cm.height is used to represent the pier model. Pressure tappings on the surface of pier plate and wall plate along the line of symmetry were connected to manometers. A blower having gradual contraction with a rectangular opening of 5 cm. x 1 cm.was fixed at a distance of 46 cm from the pier plate as shown in Fig. (2.1). The vertical position of the blower can be adjusted by the screw-jack. Maximum velocity of the jet at the opening of the blower was 67 m/s. The vertical position of the jet was changed for each experimental set up.

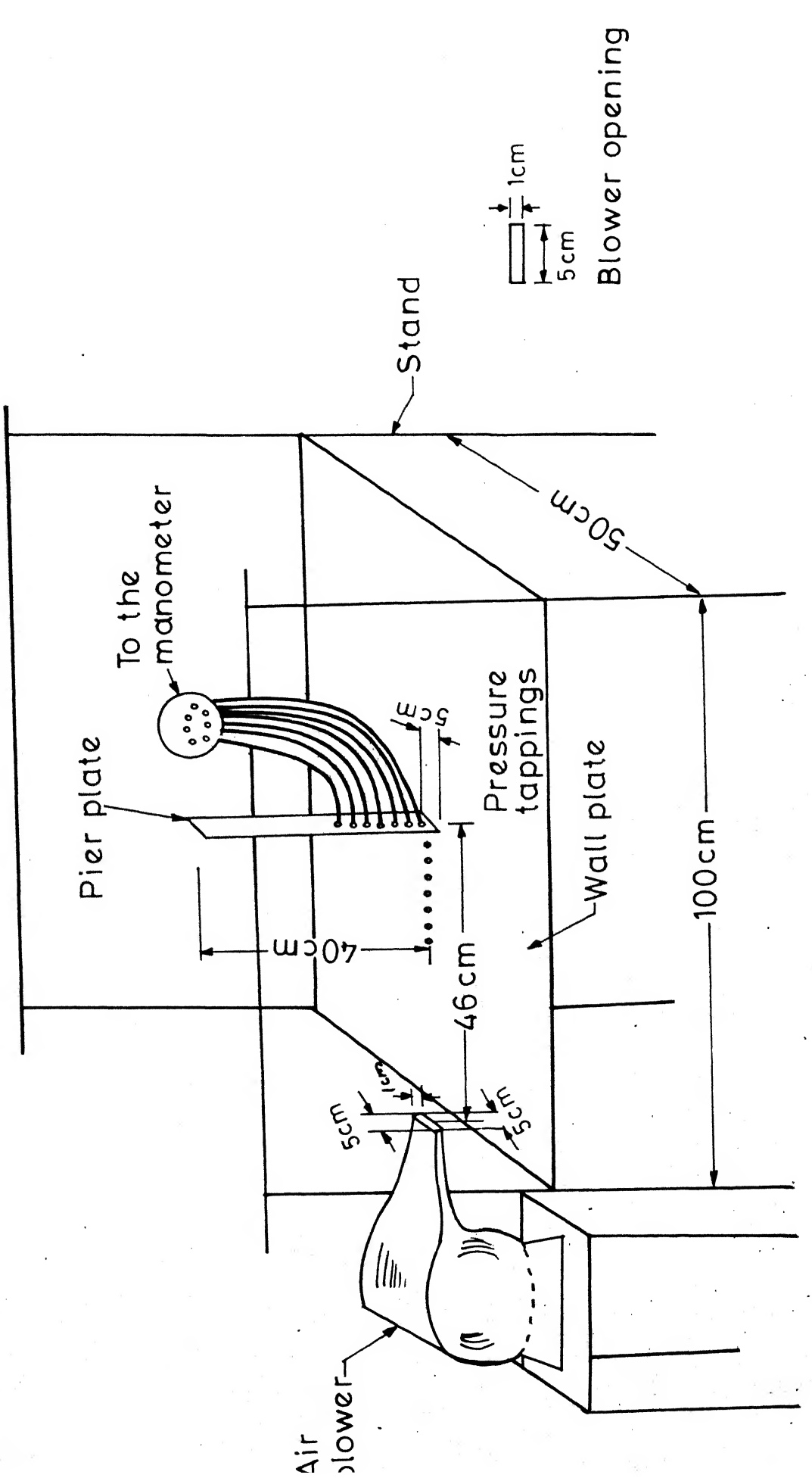

Fig.2.1 Experimental setup

2.3 Details of Measurements:

The pressure distribution on the wall and the pier plate was observed at different vertical positions of the blower from the wall as shown in Fig.(2.2). Depressions on the pressure distribution reflect the presence of the horse shoe vortex. Well defined depressions in the pressure distribution on wall were seen for blower height h_c varying from 2.5 cm to 6.5 cm. Hence the blower position was varied in the present experiment for values of h_c equal to - 3 cm, 4 cm, 5 cm, 6 cm. and 7 cm. For each position of blower, pressure, velocity and vorticity were measured on the line of symmetry in the vortex zone.

In the present study a Cartisian coordinate system (x, y, z) has been used: x, the streamwise coordinate, is measured from the origin (at the intersection of the rectangular pier and the wall on which the pier is mounted) in a down stream direction; y is measured from the origin in a direction perpendicular to the wall; z is measured from the origin which is consistent with the directions of x and y and the right hand rule. (See the figure below).

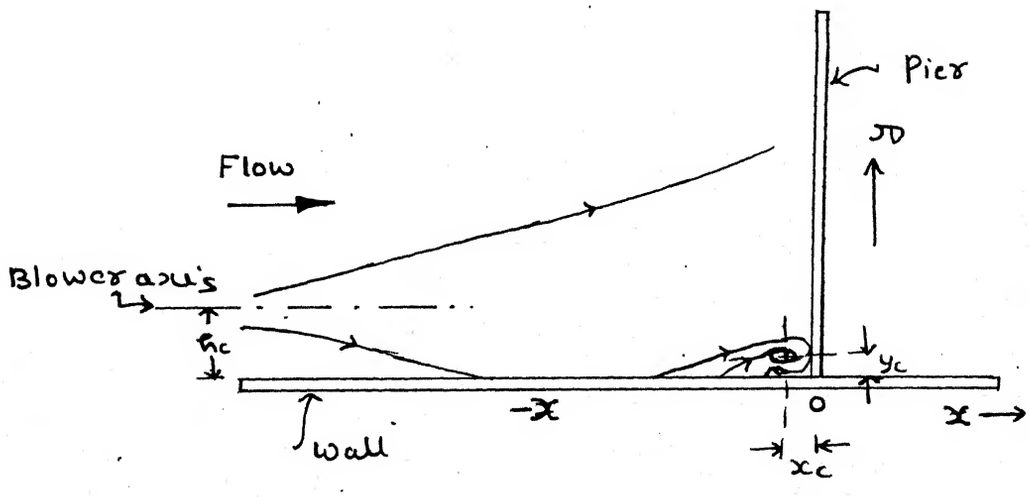

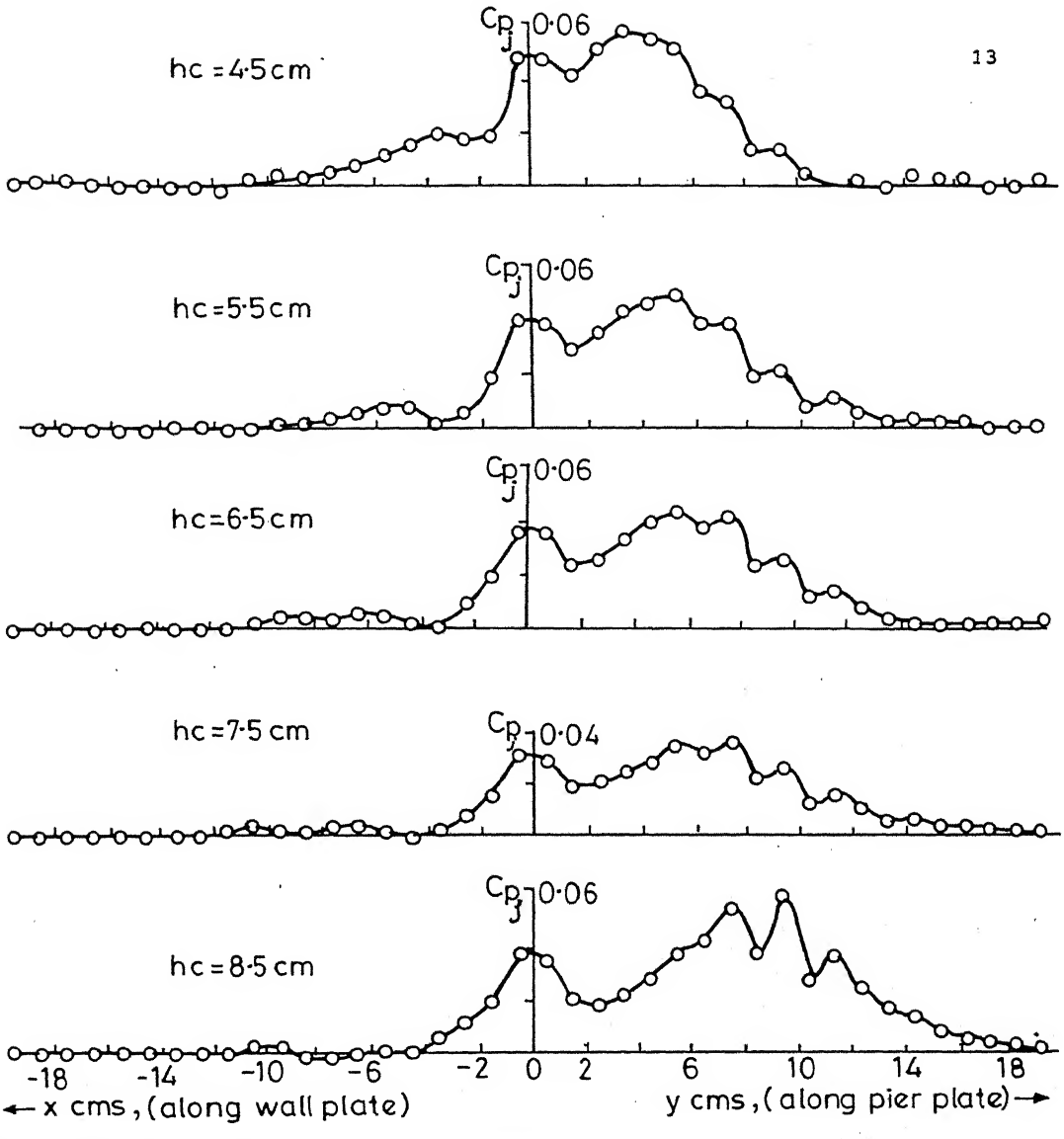

Fig.2·2 Pressure distribution on the wall plate and pier plate along the line of symmetry for different vertical positions of blower. C_{p_j} is based on jet velocity, Uj

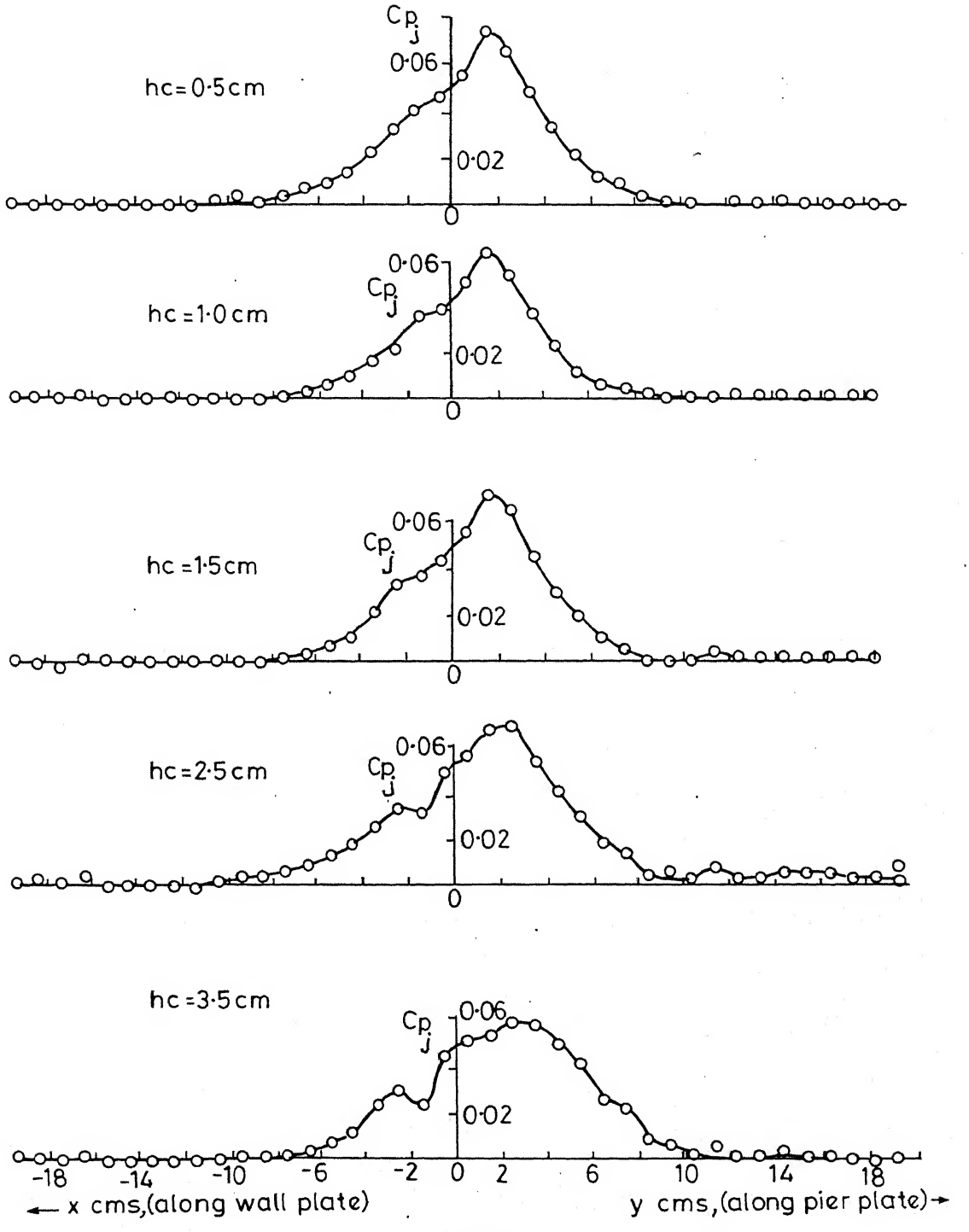

F ig. 2·2 (Continued)

The tuft survey was carried out to locate the approximate position of the vortex zone. The Kiel probe is used to measure the total pressure head. The details of the Kiel probe dimensions are shown in Fig. 2.3(a). The Kiel probe was fixed to traverse with protractor in such a way that Kiel probe can be rotated in vertical plane from 0^{o} to 180^{o}. It was placed on the line of symmetry and rotated in such a way that the pressure reading was maximum. Both the pressure and the orientation of the probe in terms of angle to the horizontal plane were recorded. This way the velocity distribution was measured on the line of symmetry both inside and outside of the separating region. Total pressure head measurement were carried out above the centre line of the jet.

The details of static probe are shown in Fig.2.3(b). The static probe was placed exactly at the position of the Kiel probe and was oriented in the direction indicated by Kiel probe. The static pressure was recorded with reference to atmospheric pressure. The difference of total head and static pressure head was used for computation of velocity.

Details of the vorticity probe used in the experiment are shown in Fig. (2.3c). The vanes are made of very thin foil so that their inertia is the minimum possible. The friction at the hinges has been reduced to its minimum. The number of rotations per minute (rpm) made by vane assembly (rotor) were measured by using the vorticity probe by synchronising the stroboscope light with the rotating vanes. These observations were made by different persons to avoid personal errors. The values agreed upon by more than two persons, were considered for the analysis.

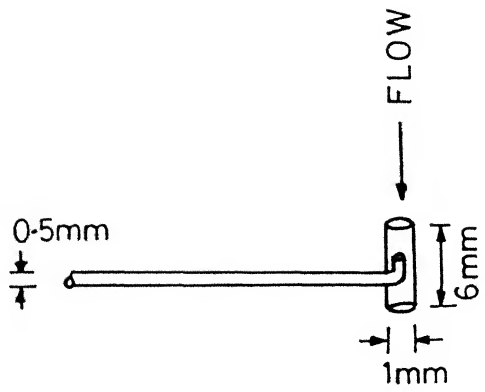

KIEL PROBE

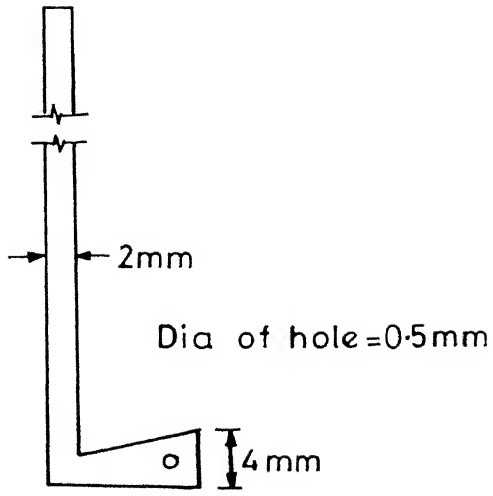

WEDGE PROBE

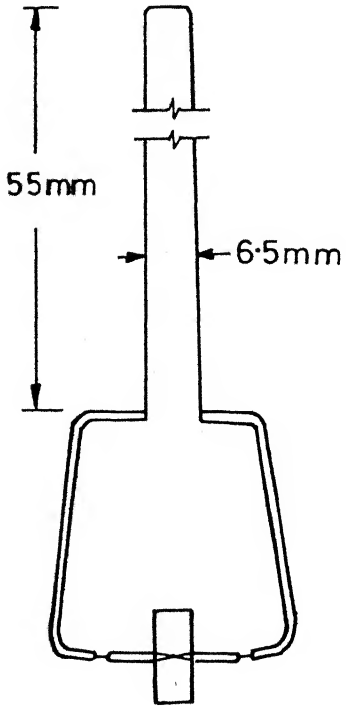

VORTICITY PROBE

Size of one vane 3x5 mm

Dia. of axis about which two vane assembly rotates = 0·3 mm

Dia of peripherial rod = 1mm

FIG. 2·3 DETAILS OF VARIOUS PROBES

2.4 Flow Visualization:

To locate the position of separating zone on the wall in front of rectnagular plate, the paint impression method was used. The wall plate was painted with white paint and dried. The wet point was first placed at the front corner of the pier and flow was started. This paint flowed according to the flow pattern in near zone of the plate. Then the paint was placed on the wall before the separating zone. Again, the flow was started. This paint flowed to indicate the line of separation. Vortices, between the line of separation and vortex zone at the front corner of the plate, were traced by using drops of different coloured paints. The drops flowed according to the flow pattern indicating the presence of vortices. Typical flow patterns have been shown in Figs. 2.4(a) to 2.4(e). The pier plate was removed for the measurement of velocity at its location. The maximum and average velocity measured at this section, in absence of the pier plate, were used for the analysis.

2.5 Flow Characteristics at the Position of Pier in the Absence of Pier:

The pier was removed from its position for the measurement of velocity distribution of undisturbed flow at pier location. Velocity round wall pressure were measured for all the blower positions under consideration are carried out. Using these measurements, the bed shear velocity, V_*, displacement thickness, $_*$, mean velocity of the flow below the centre line of the blower or upto the height of maximum velocity, and magnitude of maximum velocity were computed. The detailed velocity distributions are shown in the Figs. 2.5(a) to 2.5(e). These computed quantities

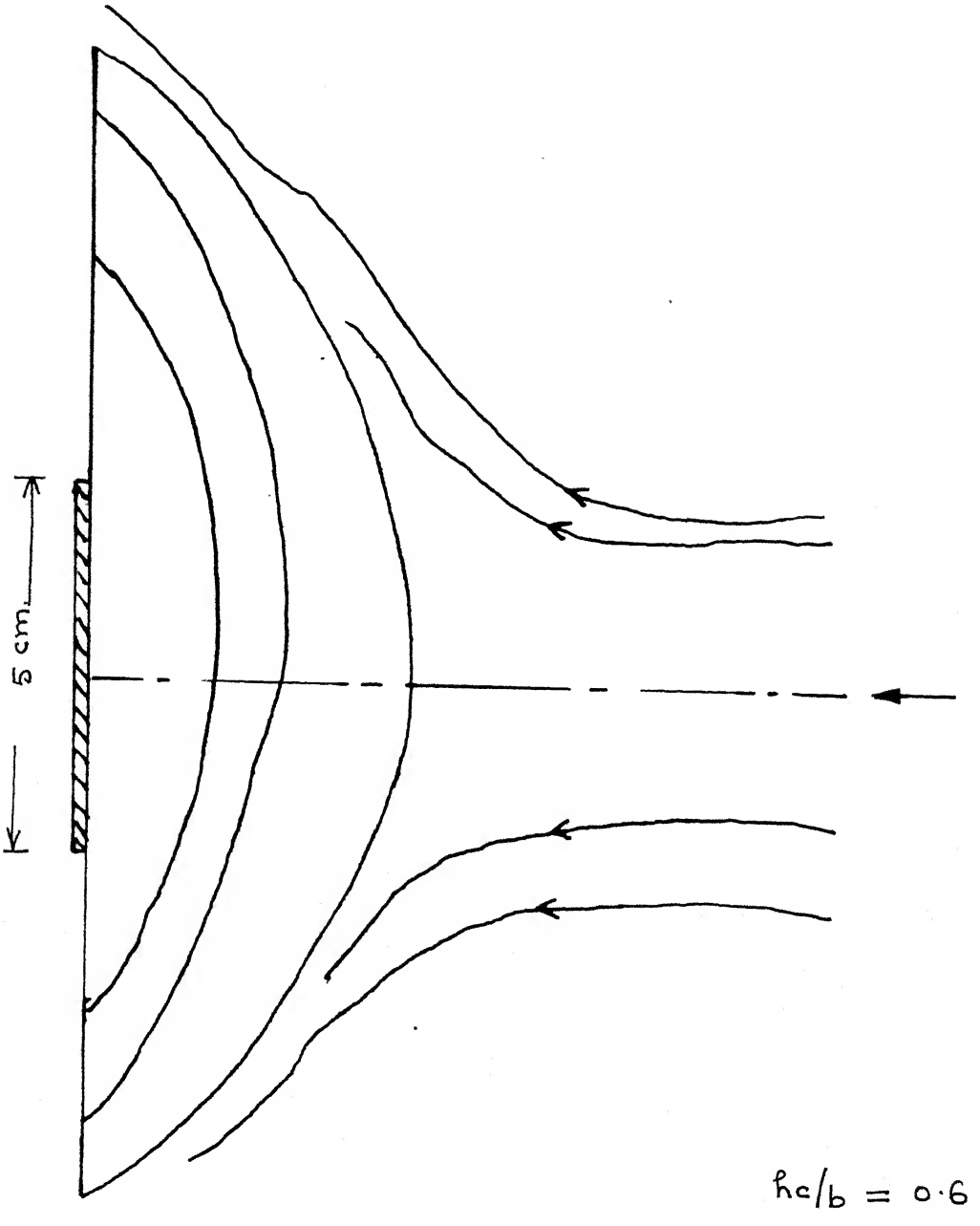

Fig. 2.4(a): Paint Impression of Flow Separation on the wall

Fig. 2.4(a): Paint Impression of Flow Separation on the Wall

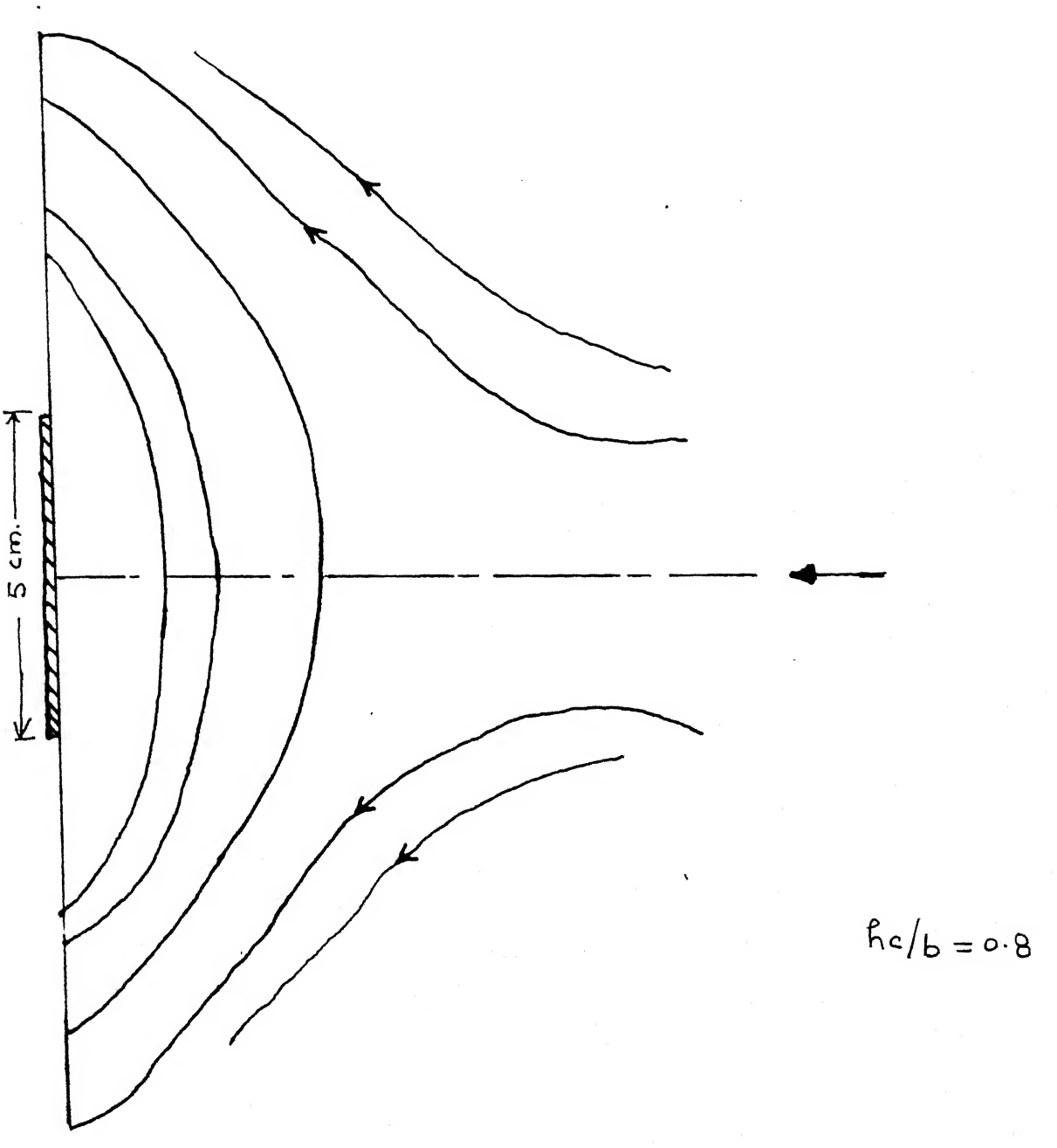

Fig. 2.4(b): Paint Impression of Flow Separation on the Wall

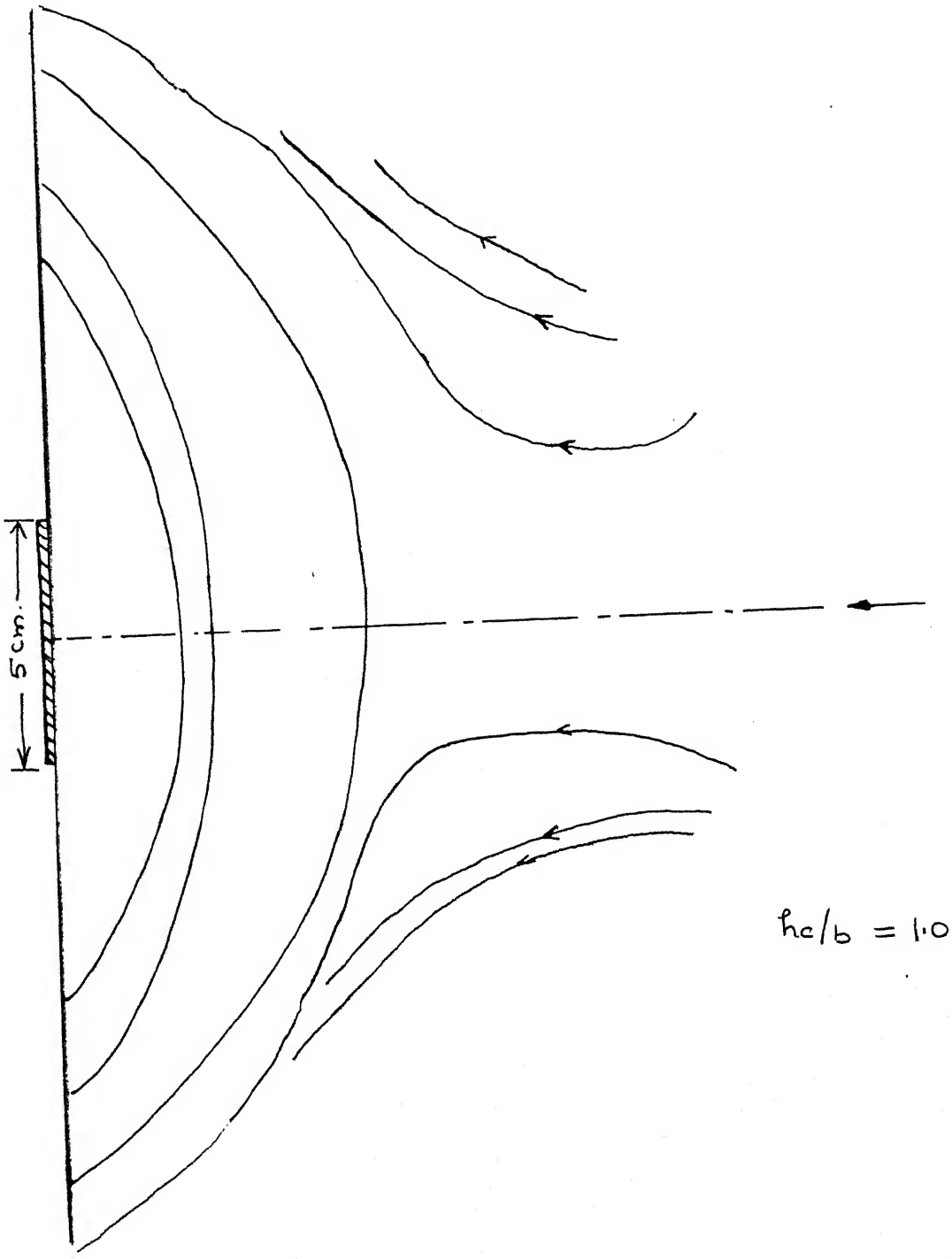

Fig. 2.4(c) : Paint Impression of Flow Separation on the Wall

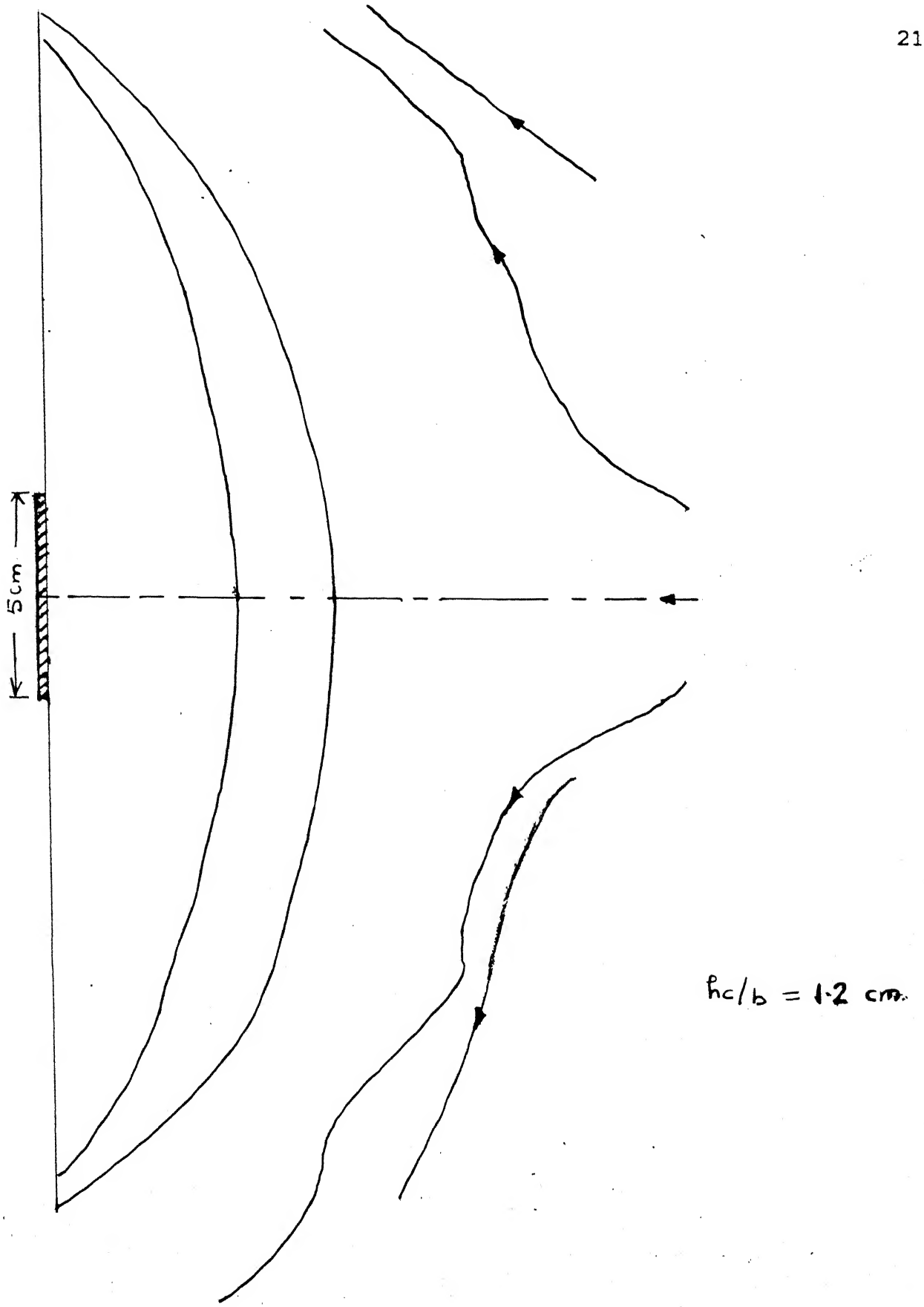

Fig. 2.4(d): Paint Impression of Flow Separation on the Wall

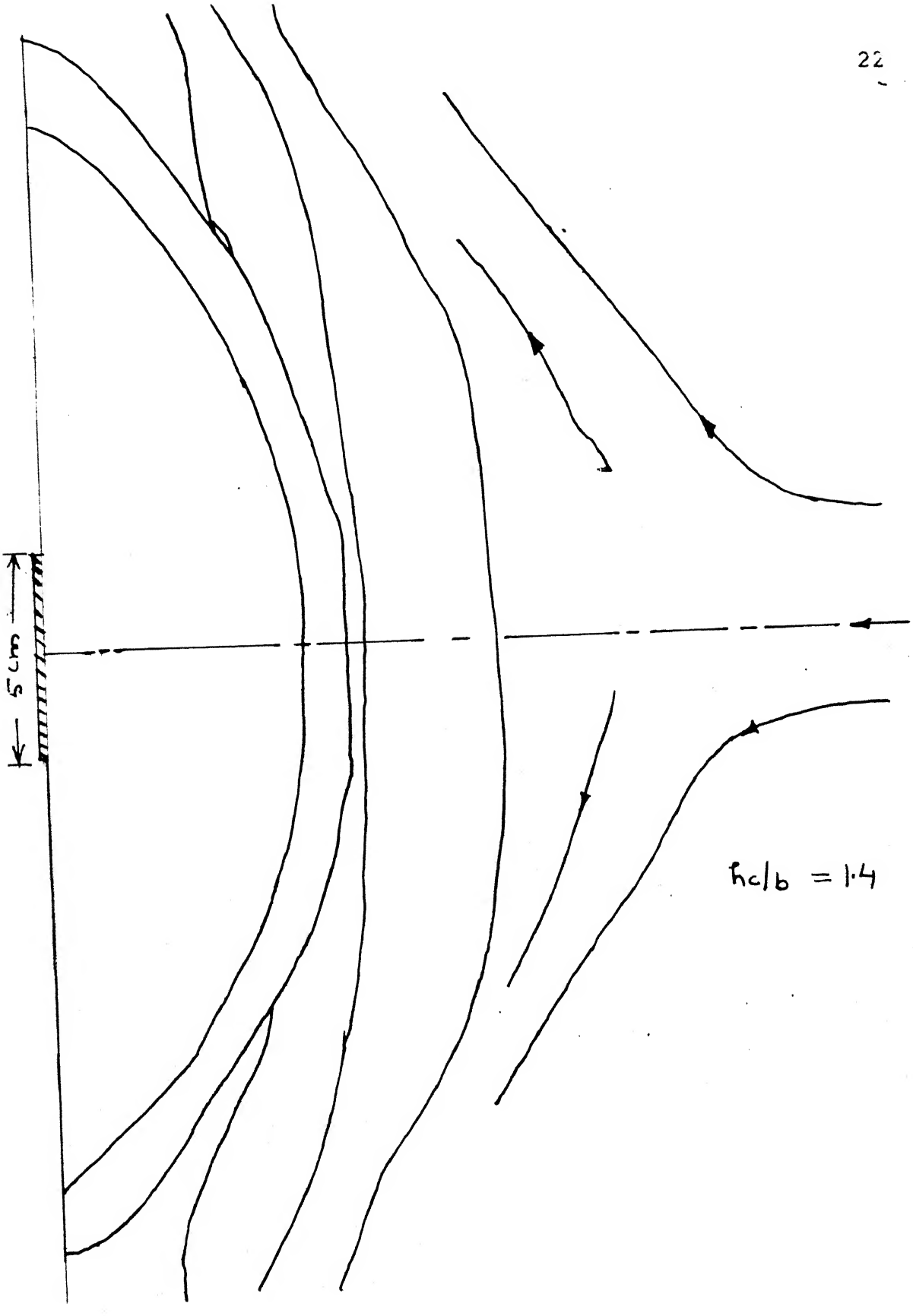
5 cm
hc/b = 1.4

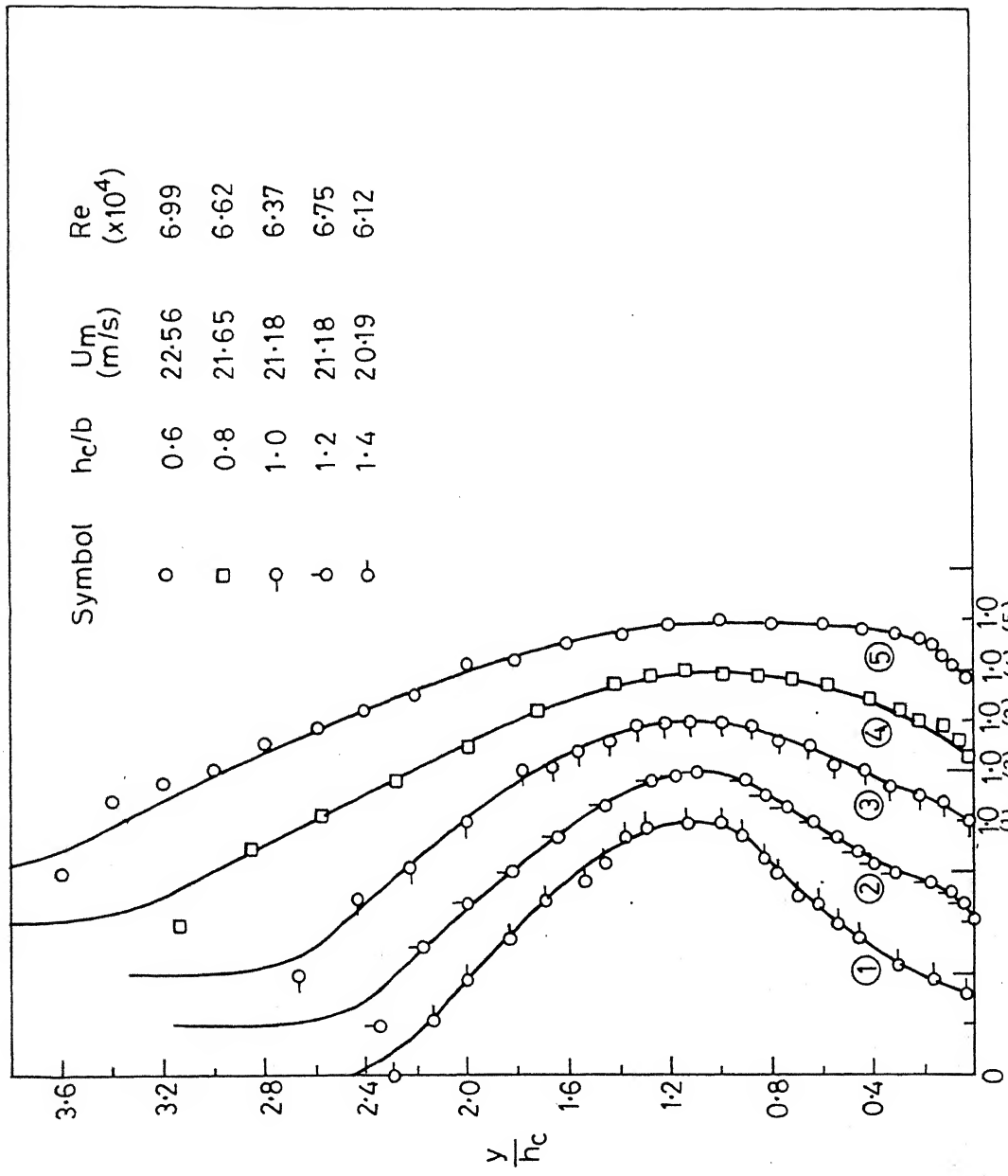

Fig.25(a) Vertical velocity distribution at the position of pier without pier plate

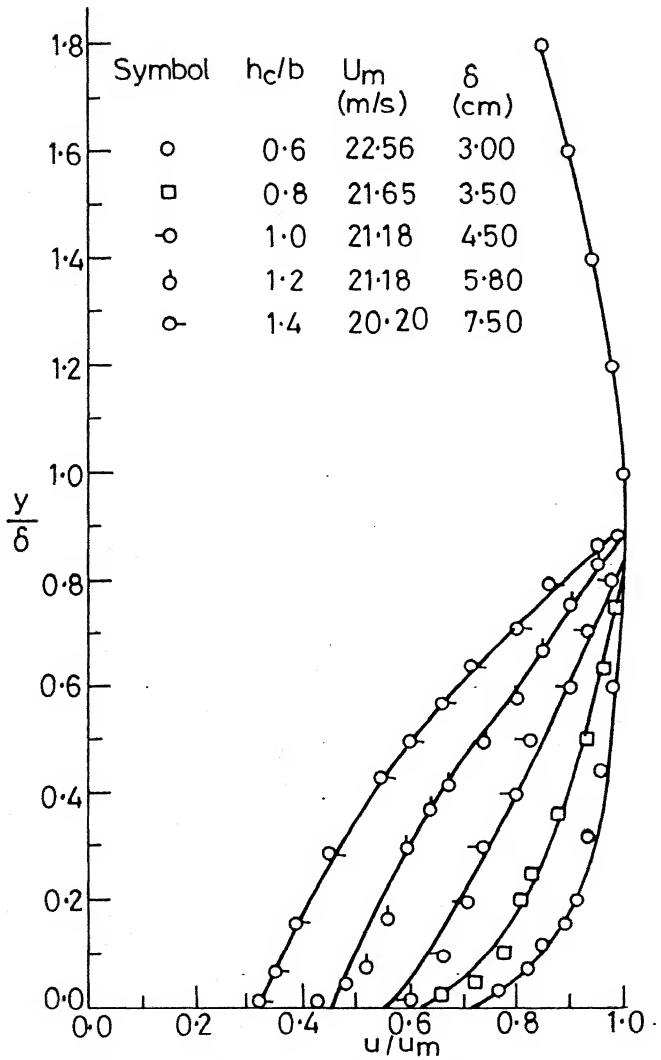

Fig.25(b)Velocity distribution in the position of pier in the absence of pier

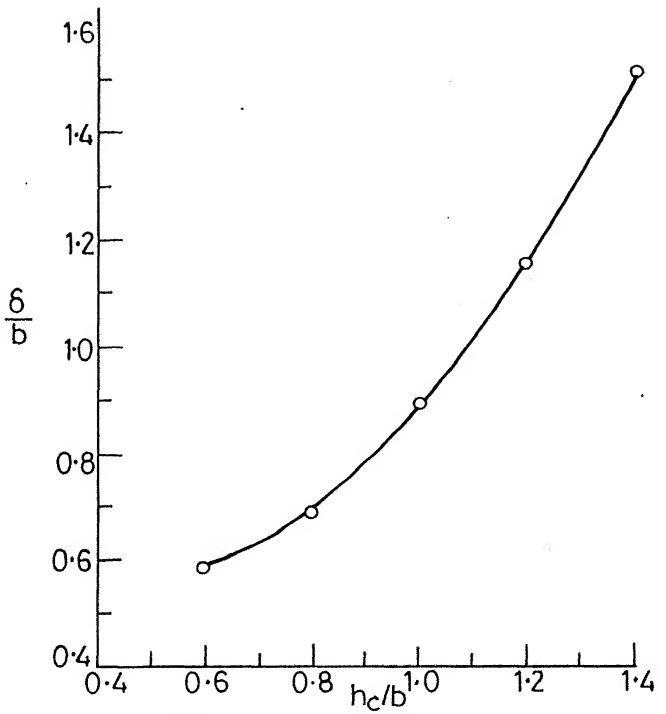

Fig.25(c)Boundary layer thickness variation

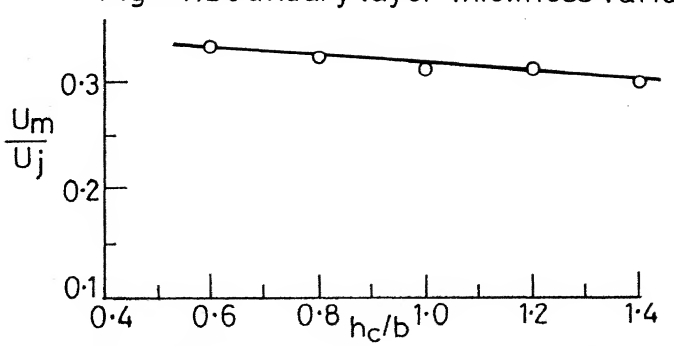

Fig.25(d)Maximum velocity decay

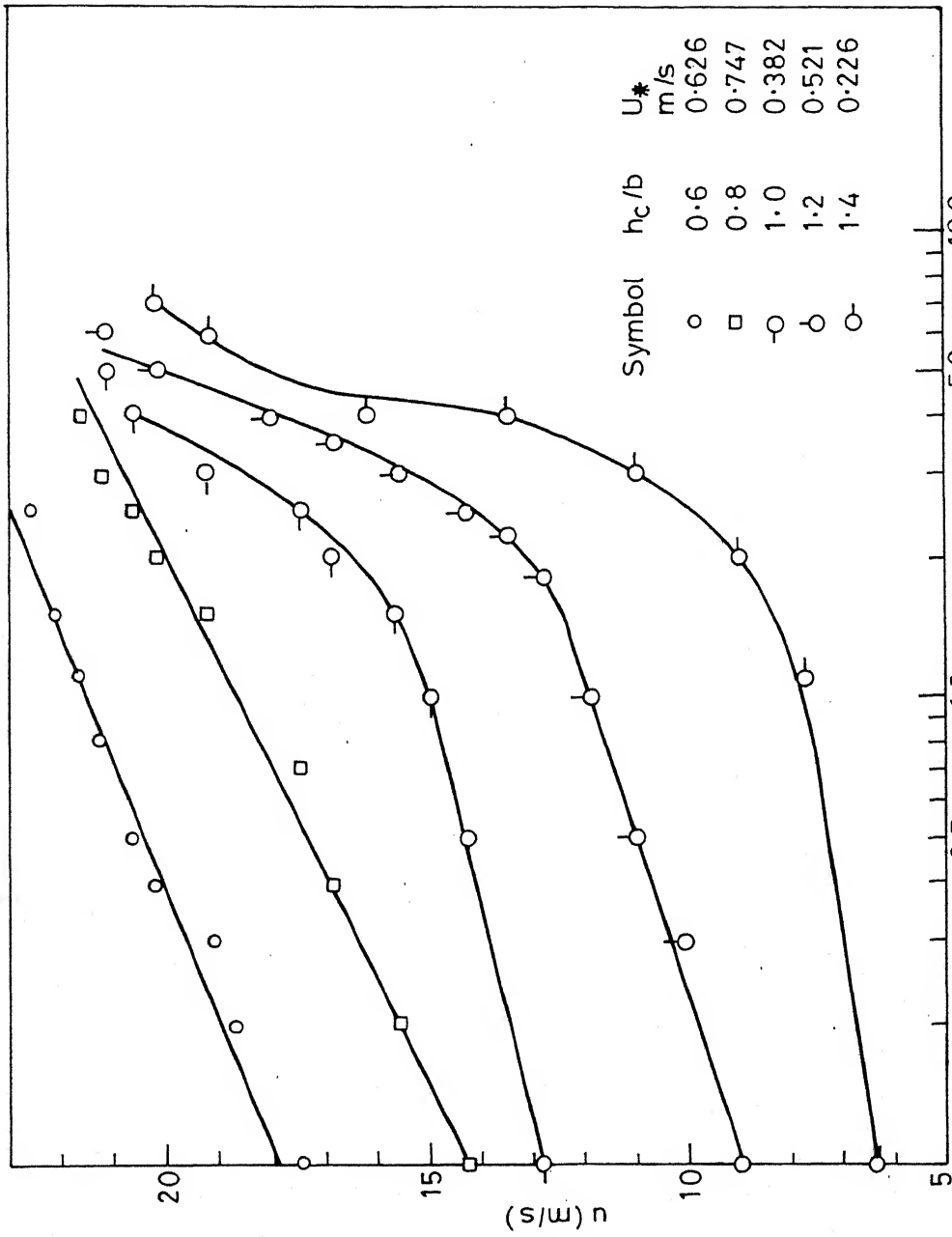

Fig.25(e)Velocity distribution in the wall region

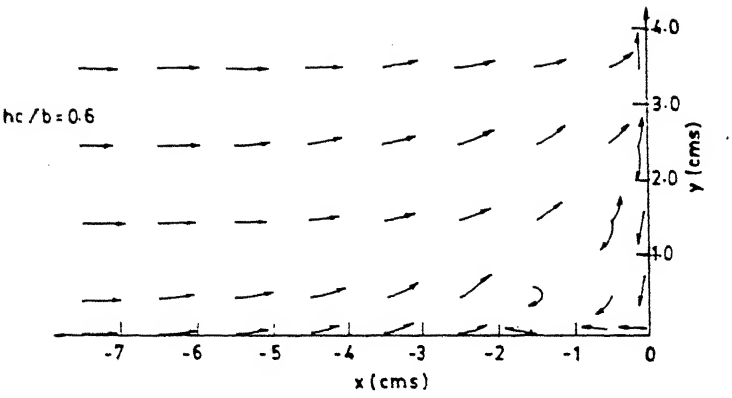

TUFT SURVEY INDICATING THE DIRECTIONS OF FLOW

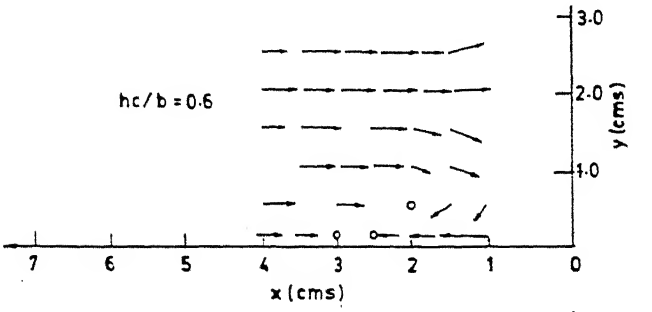

VELOCITY VECTOR DIAGRAM

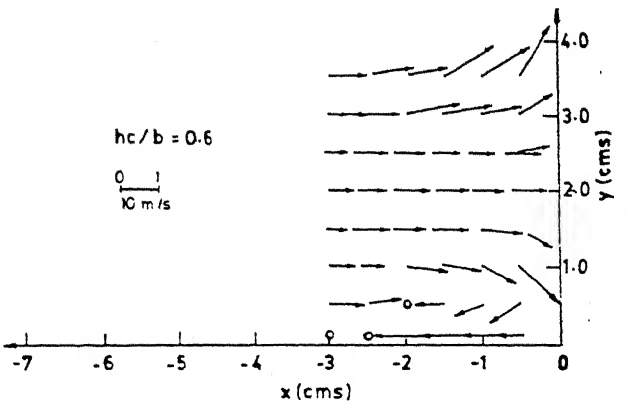

TOTAL HEAD DIAGRAM

FIG. 2.6(a) DETAILS OF VELOCITY AND PRESSURE ALONG THE LINE OF SYMMETRY IN VORTEX ZONE

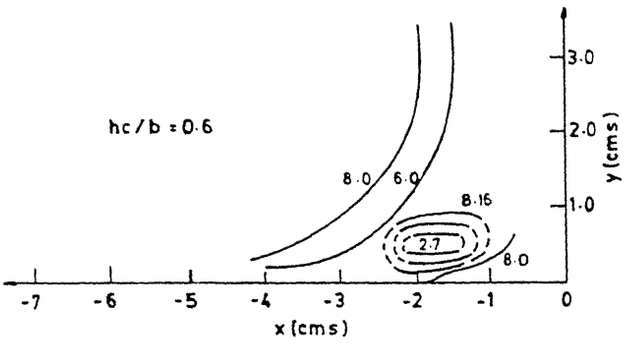

VELOCITY CONTOURS

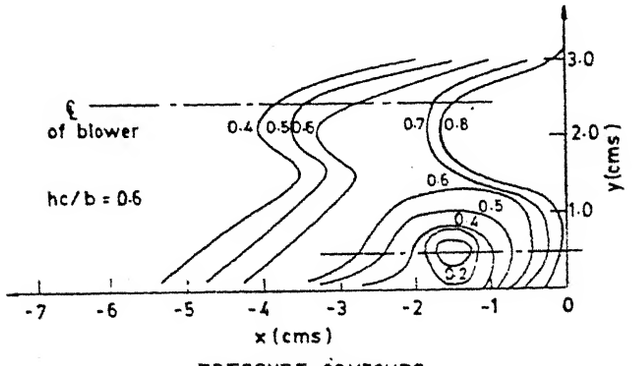

PRESSURE CONTOURS

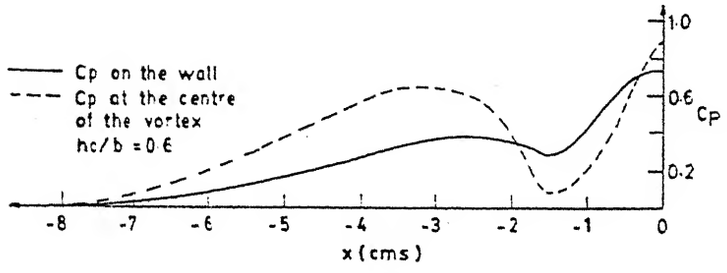

PRESSURE COEFFICIENT CURVES

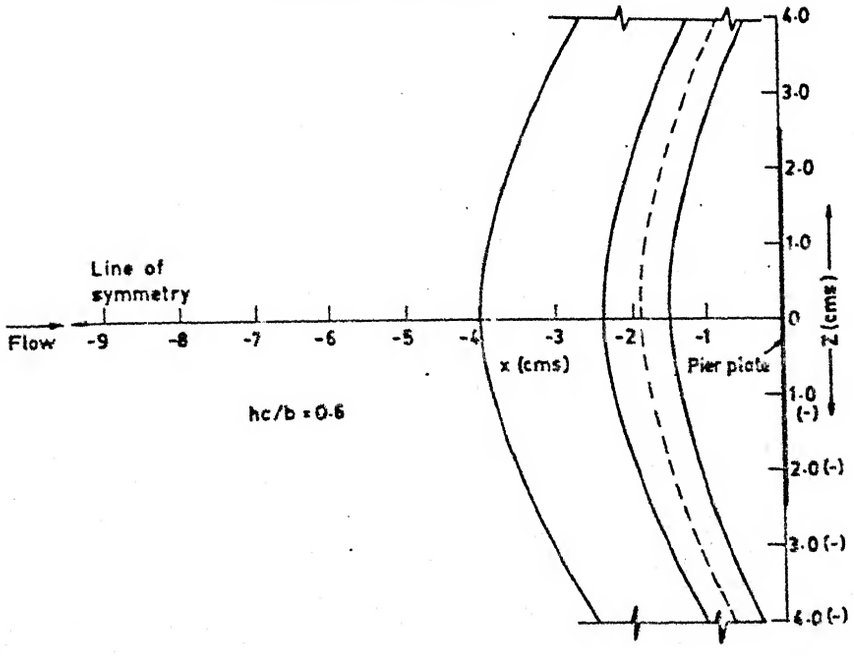

PLAN FORM OF SEPARATING REGION

FIG.2.6 CONTD.

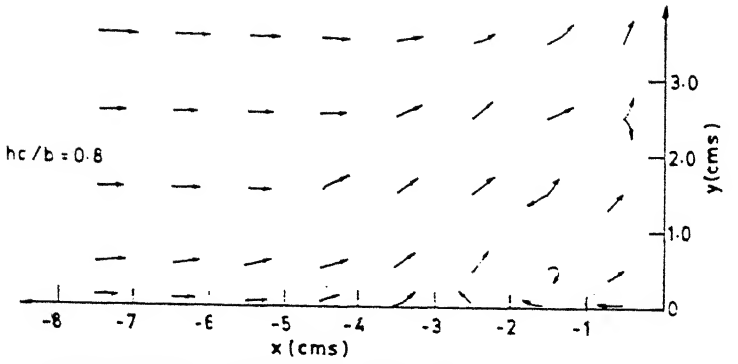

TUFT SURVEY INDICATING THE DIRECTIONS OF FLOW

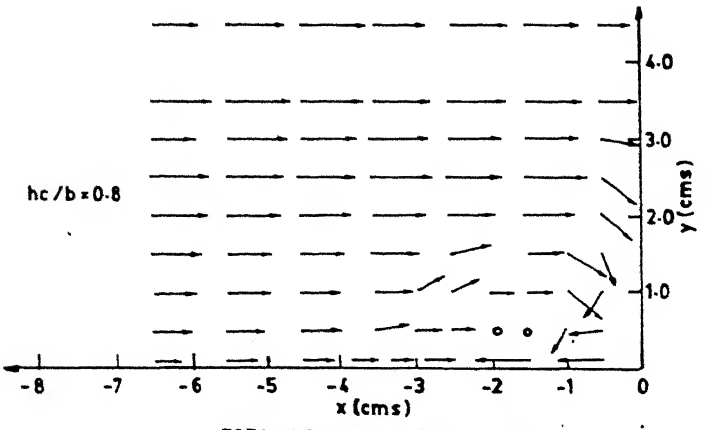

TOTAL HEAD VECTOR DIAGRAM

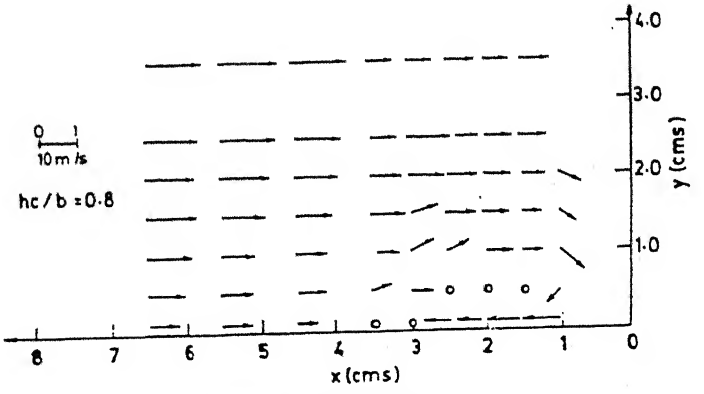

VELOCITY VECTOR DIAGRAM

FIG. 2.6(b) DETAILS OF VELOCITY AND PRESSURE ALONG THE LINE OF SYMMETRY IN VORTEX ZONE

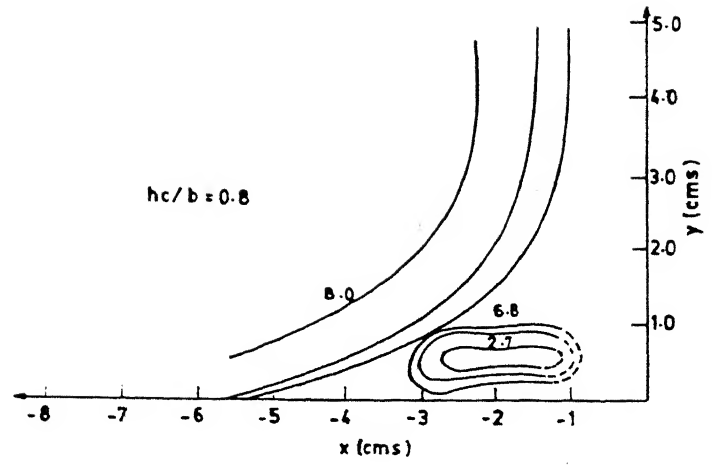

VELOCITY CONTOURS

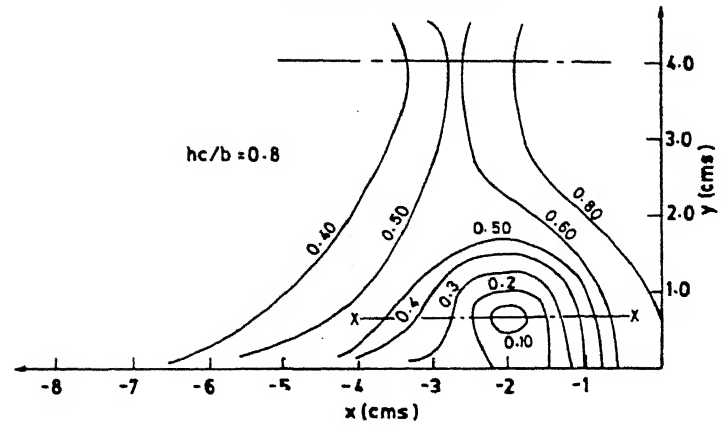

PRESSURE CONTOURS

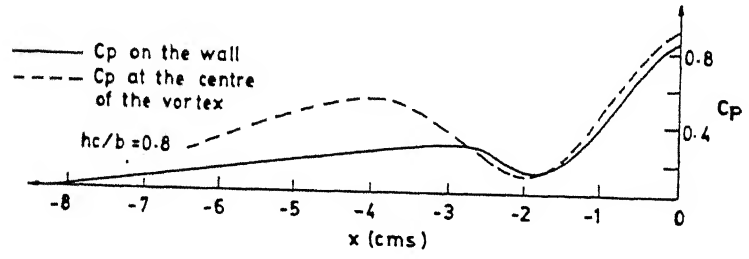

PRESSURE COEFFICIENT CURVES

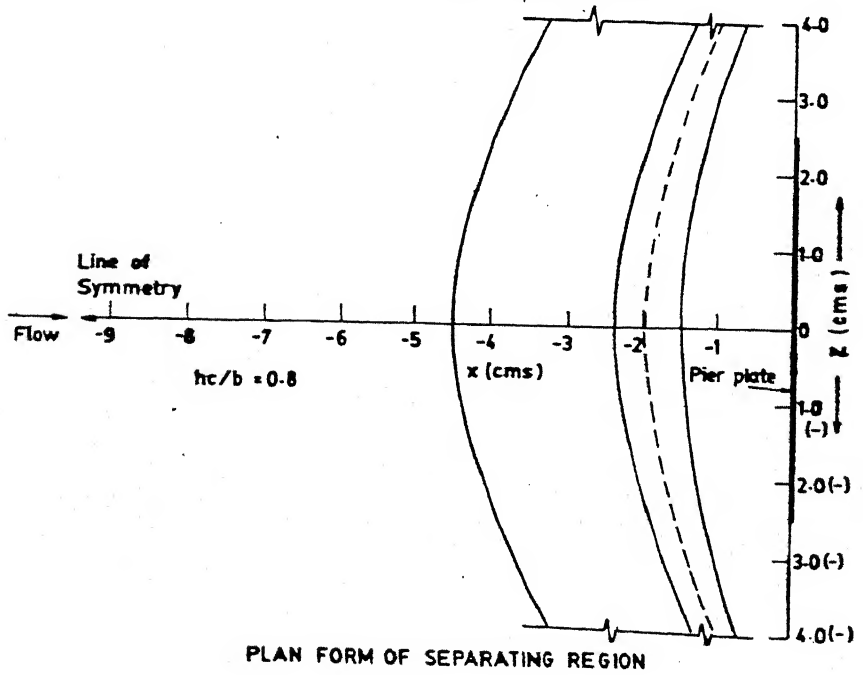

PLAN FORM OF SEPARATING REGION

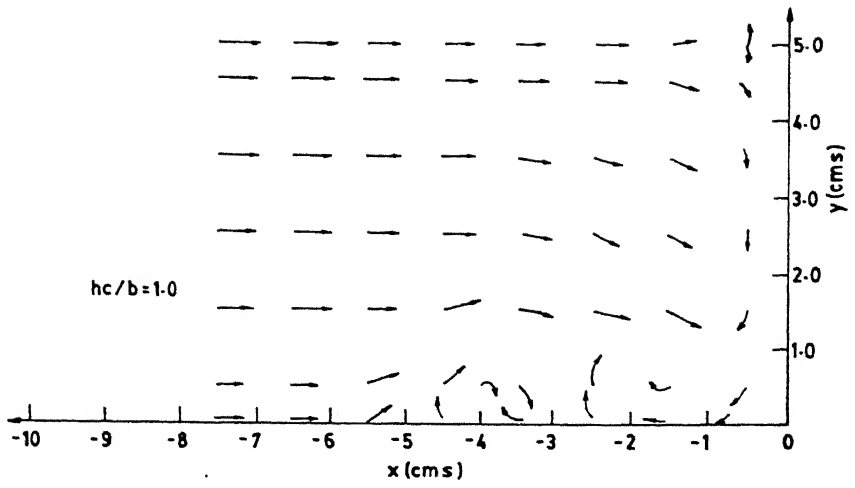

TUFT SURVEY INDICATING THE DIRECTIONS OF FLOW

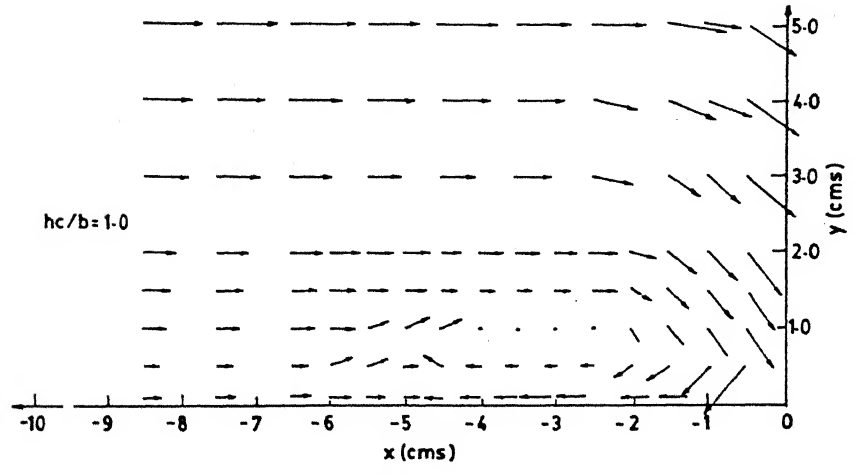

TOTAL HEAD VECTOR DIAGRAM

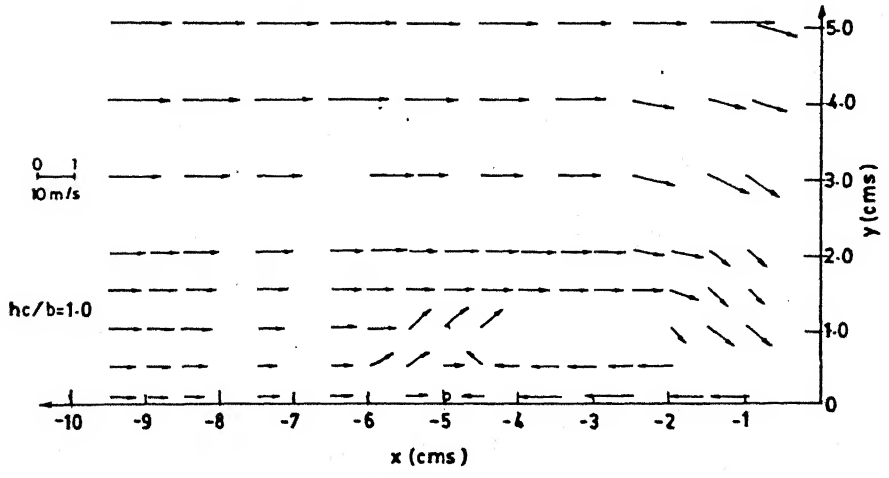

VELOCITY VECTOR DIAGRAM

FIG. 2.6(c) DETAILS OF VELOCITY AND PRESSURE ALONG THE LINE OF SYMMETRY IN VORTEX ZONE

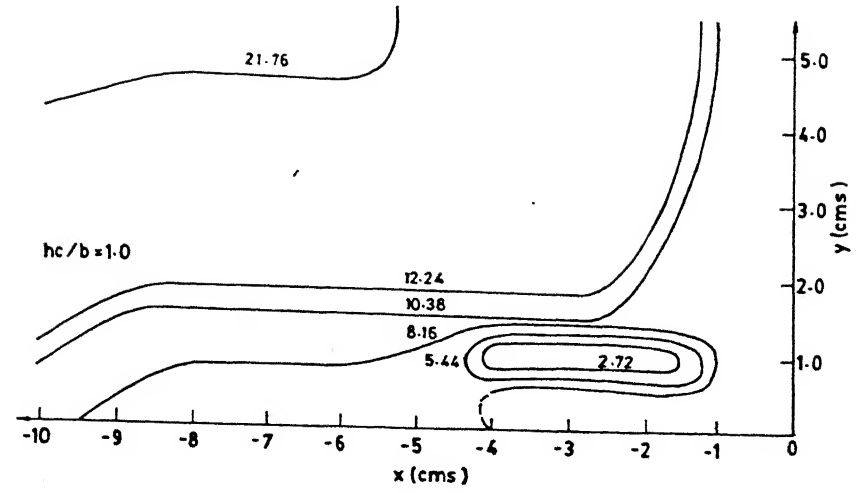

VELOCITY CONTOURS

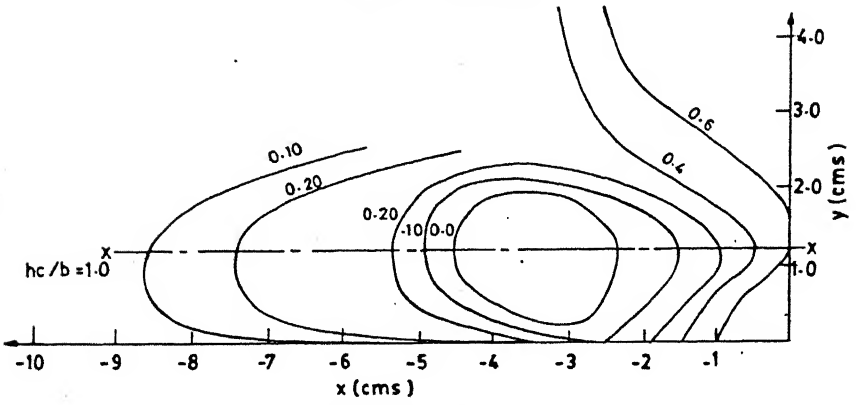

PRESSURE CONTOURS

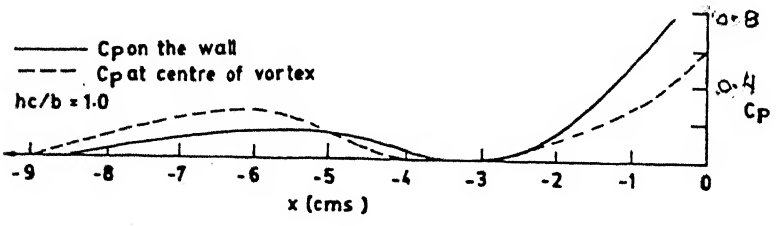

PRESSURE COEFFICIENT CURVES

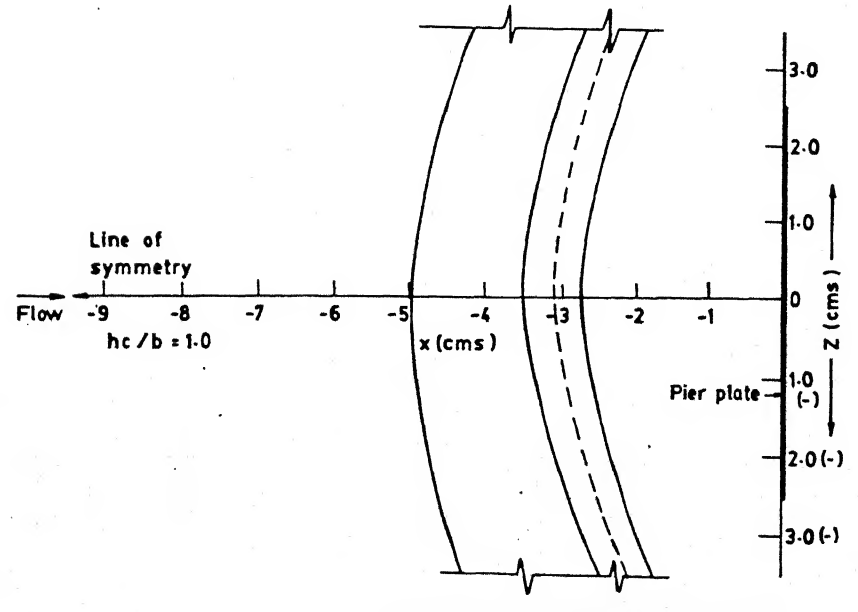

PLAN FORM OF SEPARATING REGION

FIG. 2·6(c) CONTD.

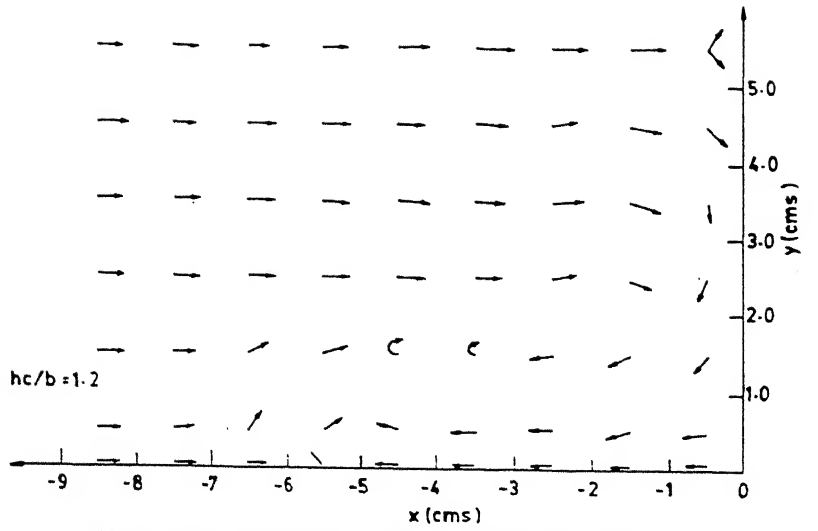

TUFT SURVEY INDICATING THE DIRECTION OF FLOW

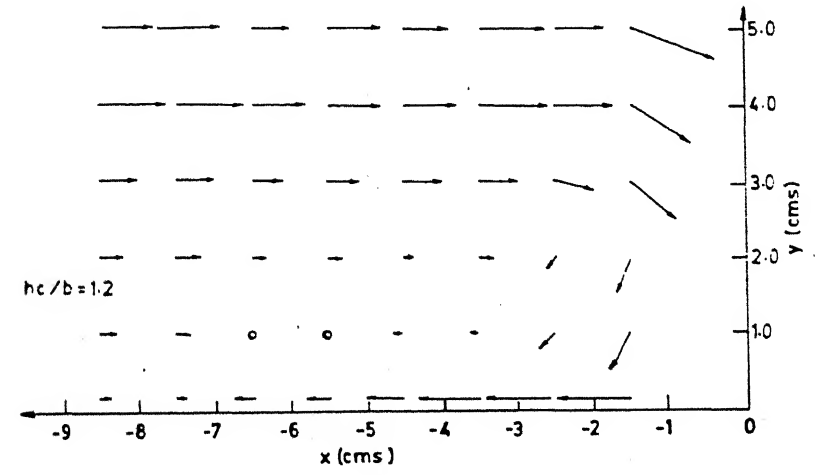

TOTAL HEAD VECTOR

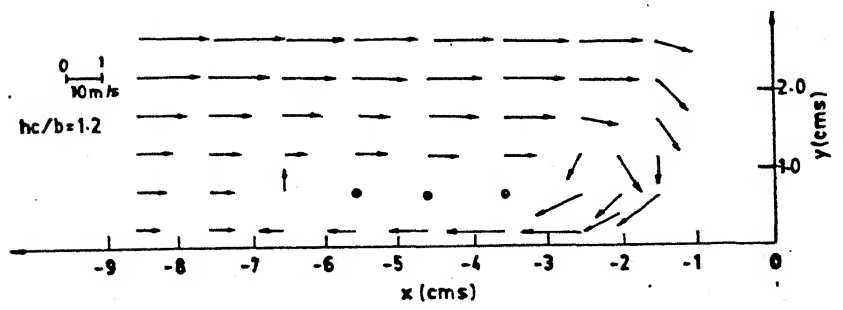

VELOCITY VECTOR DIAGRAM

FIG. 2.6 a DETAILS OF VELOCITY AND PRESSURE ALONG THE LINE OF SYMMETRY IN VORTEX ZONE

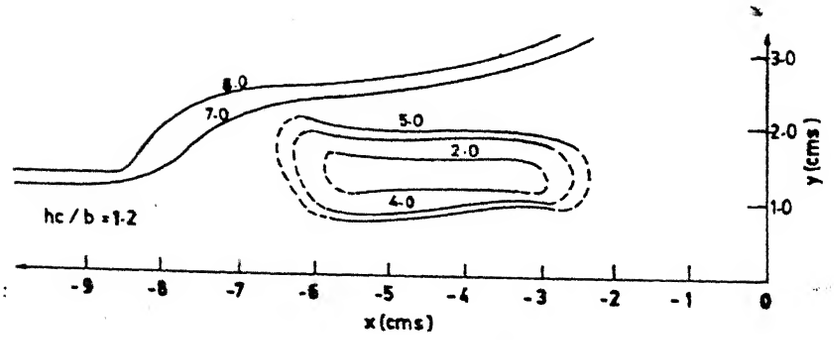

VELOCITY CONTOURS

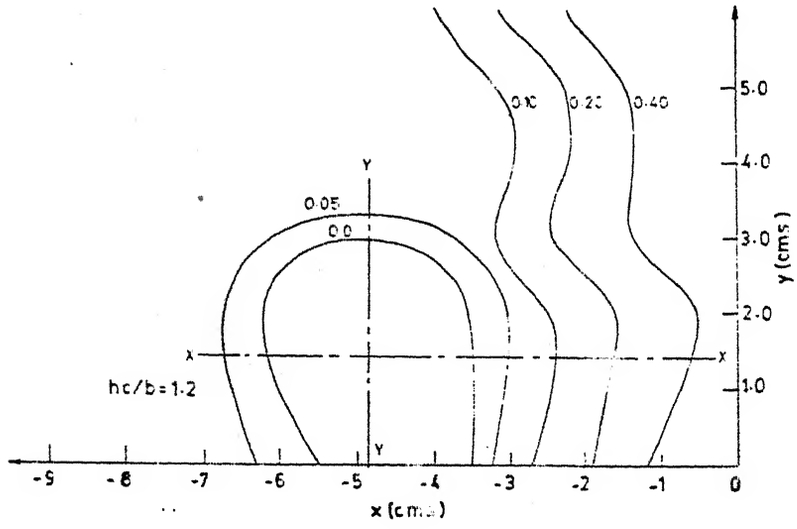

PRESSURE CONTOURS

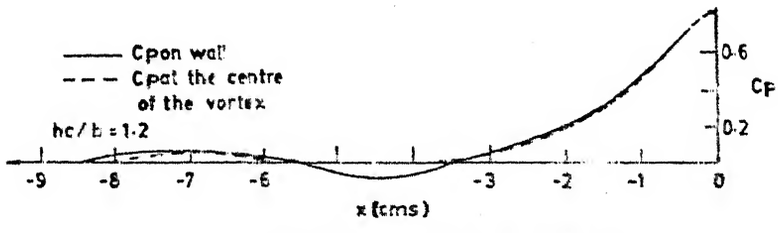

PRESSURE COEFFICIENT CURVES

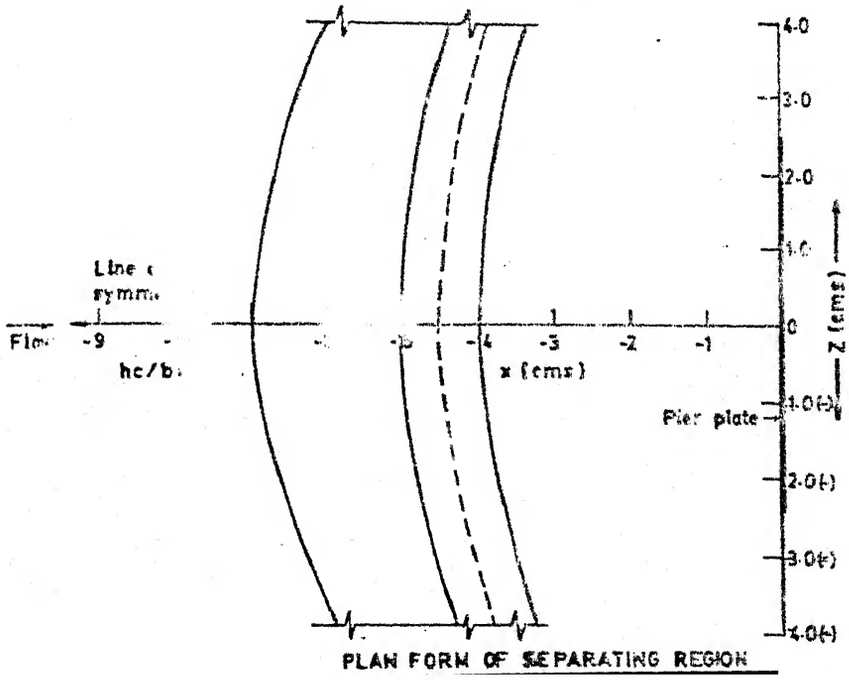

PLAN FORM OF SEPARATING REGION

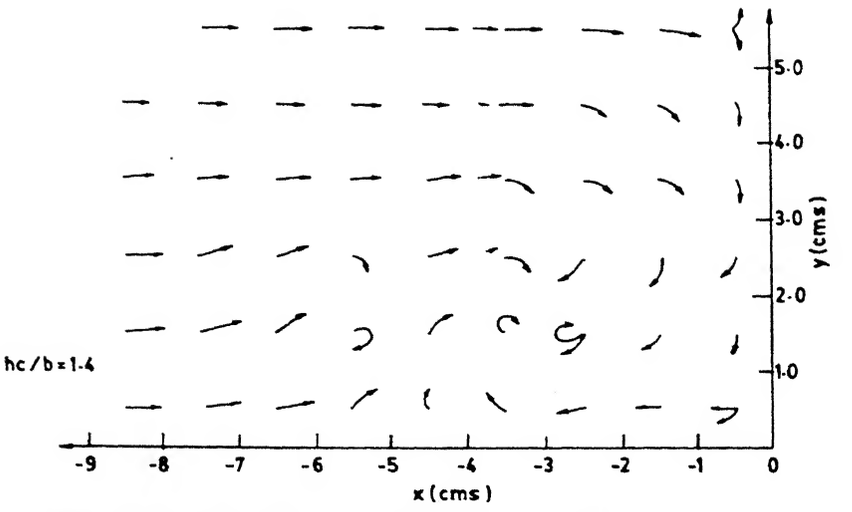

TUFT SURVEY INDICATING THE DIRECTIONS OF FLOW ALONG THE LINE OF SYMMETRY

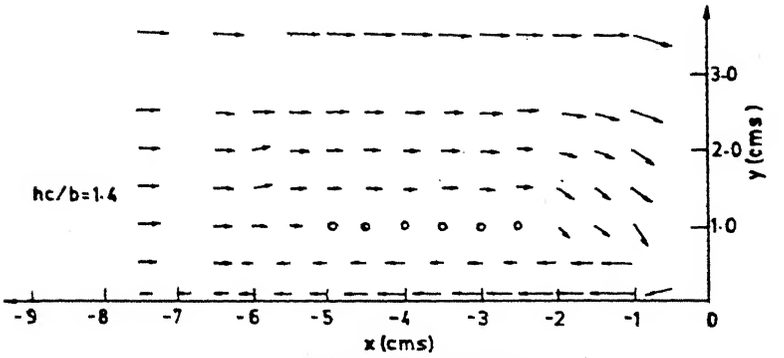

TOTAL HEAD VECTOR

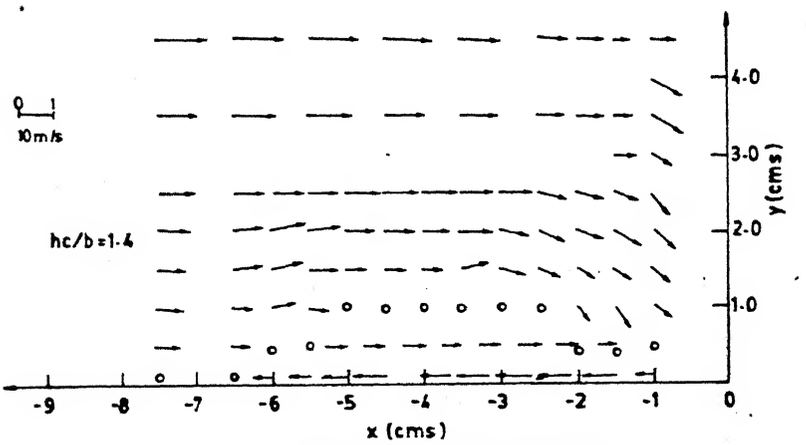

VELOCITY VECTOR DIAGRAM

FIG. 2.6(e) DETAILS OF VELOCITY AND PRESSURE ALONG THE LINE OF SYMMETRY IN VORTEX ZONE

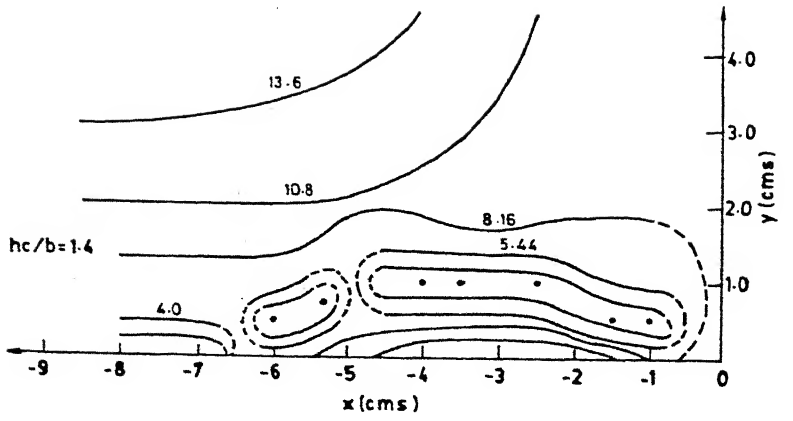

VELOCITY CONTOURS

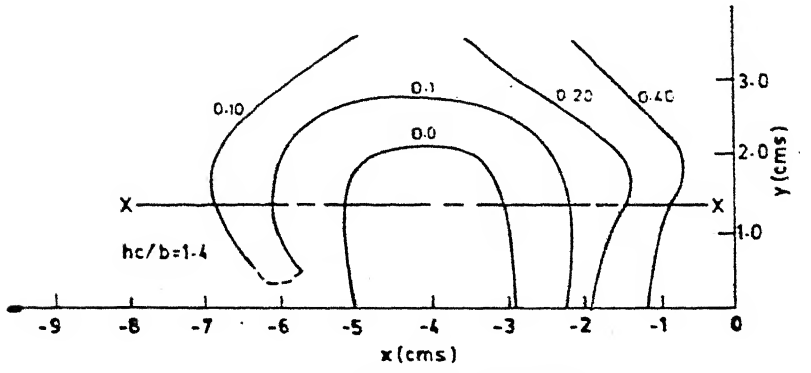

PRESSURE CONTOURS

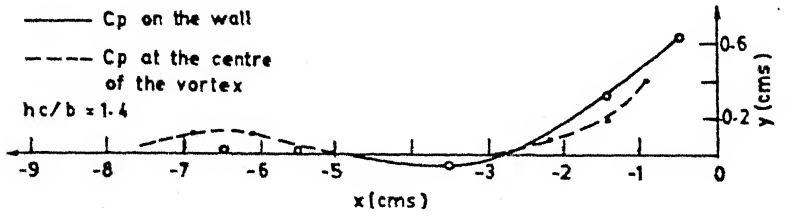

PRESSURE COEFFICIENT CURVES

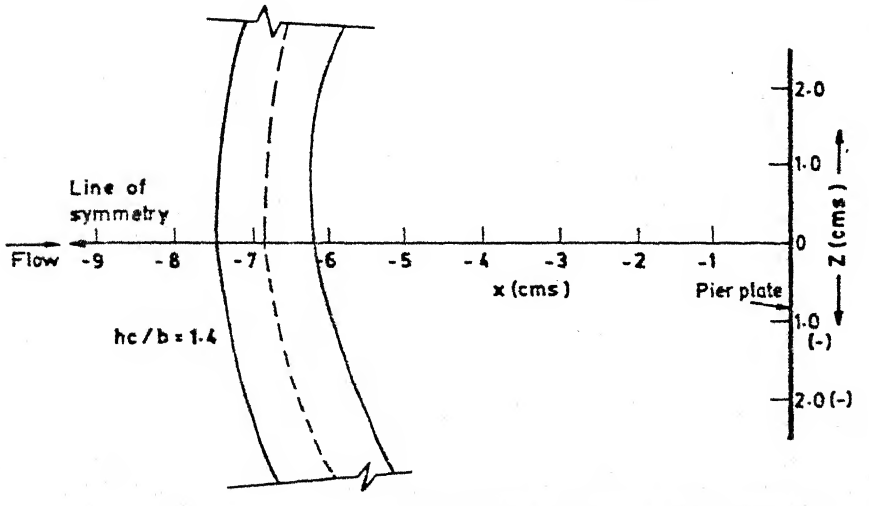

PLAN FORM OF SEPARATING REGION

FIG. 2.6 CONTD.
(e)

were used in the analysis of the horse shoe vortex which occurs when the pier is replaced.

2.6 Methodology for the Computation of Data:

2.6.1 Computation of Pressure Coefficient (C_p):

The pressure head ' h' at each pressure tapping is measured with respect to the undisturbed pressure on the line of symmetry far upstream of the pier plate. This pressure is non-dimensionalized using the maximum velocity 'U_m' at the pier position, measured in its absence. Pressure C_p is computed as

$$C_p = \frac{h}{h_v} \qquad (2.2)$$

where, $h_v(\gamma_w - \gamma_a) = \frac{1}{2} \rho_a U_m^2$

suffix 'w' indicates water

'a' indicates air

m' indicates maximum value

and γ is unit weight

' h' indicates static pressure head on wall

h_v' indicates velocity head (maximum) for undisturb flow.

Figures 2.6(a) to 2.6(e) indicate the tuft survey, velocity vectors, total head contours, velocity contours, static pressure contours and static pressure distribution on the wall for each set of the vertical position of the blower.

2.6.2 Computation of Vortex Strength:

From velocity contours: Isovels of the maximum tangential velocity 'V_θ' which enclose the vortex are used for the computation of vortex strength designated as Γ_{V_θ} as follows:

$$\Gamma_{V_\theta} = V_\theta \cdot P_e \qquad (2.3)$$

where P_e is the perimeter of the velocity contour of maximum tangential velocity, V_θ.

The vortex strength Γ_{V_θ} is non-dimensionalized using pier width 'b' and the average velocity at pier location is computed as

$$\bar{U} = \frac{U_m(\delta - \delta_*)}{\delta} \qquad (2.4)$$

where U_m = maximum velocity of undisturbed flow and

δ and δ_* are boundary layer thickness and displacement thickness respectively. 'δ' is that of 'y' at which u=0.99 U_m

δ_* is computed from the relation

$$\delta_* = \int_0^\delta \left(1 - \frac{u}{U_m}\right) dy \qquad (2.5)$$

The non-dimensional vortex strength from velocity contour is written as

$$\Gamma^*_{V_\theta} = \frac{V_\theta}{\pi b \bar{U}} = \frac{V_\theta \; P_e}{\pi \; b \; \bar{U}} \qquad (2.6)$$

where b is width of pier.

The vortex strength is also computed from the pressure distribution. The method for computing Γ_{C_p} given by Gupta (1984) is used in this analysis. The equation for Γ_{C_p} according to Gupta (1984) is given as under

$$\Gamma_{C_p} = \frac{2r}{b} \sqrt{\Delta C_p}$$

where, '2r' is the lateral dimension of pressure depression and ΔC_p is the pressure difference between the crest and trough of the pressure distribution curve.

2.6.3 Computation of Vorticity:

The vorticity, ω, is computed from the maximum velocity

contour as follows:

$$\omega = \frac{V_\theta}{P_e} \text{ in number of rotations per second} \qquad (2.7)$$

$$\omega \text{ (in radians)} = 2\pi \frac{V_\theta}{P_e}$$

2.6.4 Size of the Horse Shoe Vortex:

The size of the vortex D_o is measured as the vertical dimension or minor axis of the velocity contour of the maximum tangential velocity which encloses the vortex as shown in Fig. below.

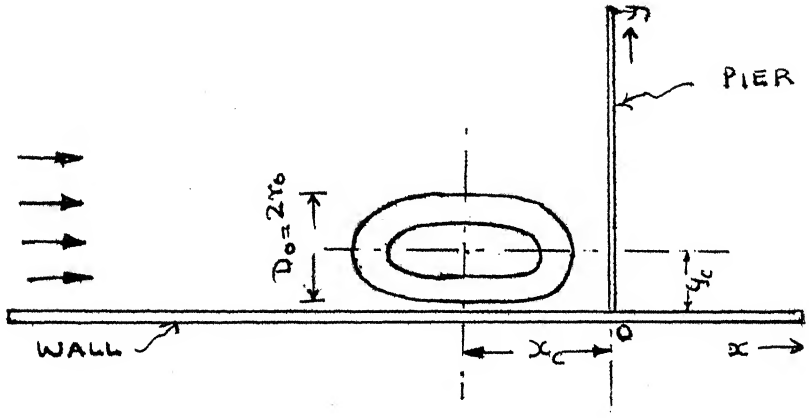

2.7 Experimental Data:

The details of the experimental data measured and computed are given in Tables 2.1, 2.2, 2.3, 2.4, 2.5, 2.6 and 2.7.

TABLE 2.1: OBSERVATIONS OF UNDISTURBED FLOW CHARACTERISTICS

h_c/b	Temp., ^oC	ν $(m^2/s) \times 10^{-5}$	U_m (m/s)	$\bar{U}$ (m/s)	U_* (m/s)	δ (cm)	δ_* (cm)
0.6	32	1.614	22.56	21.42	0.626	3.0	1.525
0.8	34	1.633	21.65	19.18	0.747	3.5	0.400
1.0	37	1.660	21.18	17.65	0.382	4.5	0.750
1.2	27	1.57	21.18	16.12	0.521	5.8	1.386
1.4	36	1.625	20.20	13.87	0.226	7.0	2.379

TABLE 2.2: COMPUTATION OF UNDISTURBED FLOW CHARACTERISTICS

h_c/b	$\frac{U_m b}{\nu} \times 10^4$	$\frac{\bar{U} b}{\nu} \times 10^4$	$\frac{U_m \delta^*}{\nu} \times 10^3$	$\frac{U_m b}{U_* \delta}$	$\frac{U_* \cdot \delta^*}{\nu} \times 10^2$
0.6	6.99	6.64	2.12	60.00	5.91
0.8	6.62	5.87	5.29	41.40	1.83
1.0	6.37	5.32	9.56	61.60	1.73
1.2	6.75	5.13	1.86	35.00	1.69
1.4	6.12	4.20	2.89	59.58	3.30

TABLE 2.3: STRENGTH COMPUTATION FROM VELOCITY DISTRIBUTION

h_c/b	P_e (cm)	V_θ (m/s)	$\Gamma_{V_\theta} = V_\theta \times P_e$ (m^3/s)	$\Gamma^*_{V_\theta} = \frac{V_\theta}{\pi b \bar{U}}$
0.6	4.00	8.16	0.3264	0.092
0.8	5.20	6.80	0.3536	0.117
1.0	7.00	5.44	0.3808	0.137
1.20	9.75	5.00	0.4875	0.193
1.4	10.25	5.44	0.5576	0.256

TABLE 2.4: STRENGTH COMPUTATION FROM PRESSURE DISTRIBUTION

h_c/b	$2\ r_\omega/b$	C_p	$\Delta C_{p\omega}$	ΔC_{pc}	$\sqrt{C^*_{cp\omega}} = \frac{2\ r}{b}\sqrt{\Delta C_{p\omega}}$	$\sqrt{C^*_{Pc}} = \frac{2}{b} r_c \sqrt{\Delta C_{pc}}$
0.6	0.5	0.6	0.26	0.72	0.256	0.509
0.8	0.6	0.8	0.34	0.60	0.349	0.581
1.0	0.8	1.2	0.22	0.40	0.375	0.759
1.2	0.9	1.2	0.18	0.24	0.382	0.657
1.4	0.9	1.2	0.30	0.38	0.44	0.739

TABLE 2.5: POSITION AND SIZE OF THE VORTEX

h_c/b	x_c (cm)	y_c (cm)	D_o (cm)	x_c/b	y_c/b	$\frac{U_m D_o}{\nu} \times 10^3$
0.6	1.50	0.50	0.80	0.30	0.10	11.180
0.8	2.00	0.65	0.75	0.40	0.13	9.940
1.0	3.00	1.00	0.80	0.60	0.24	10.200
1.2	4.50	1.30	1.00	0.90	0.26	13.490
1.4	3.75	1.00	0.75	0.80	0.20	9.320

TABLE 2.6: OBSERVATION OF VORTICITY

h_c/b	location of the probe		Observed vorticity (rpm)
	x_v (cm)	y_v (cm)	
0.6	1.75	0.5	2430
0.8	1.75	0.5	2500
1.0	3.00	1.0	2640
1.2	3.00	1.0	2650
1.4	3.00	1.0	2700

TABLE 2.7: COMPUTATION OF VORTICITY

h_c/b	V_θ (m/s)	P_e (cm)	$\omega = \frac{V_\theta}{P_e}$ rpm	$\omega_* = \frac{\omega b}{\bar{U}}$
0.6	8.16	4.00	12240	5.58
0.8	6.80	5.20	7846	4.28
1.0	5.44	7.00	4663	2.76
1.2	5.00	9.75	3077	1.99
1.4	5.44	10.25	3184	2.40

CHAPTER - 3

STRENGTH CHARACTERISTICS OF HORSE SHOE VORTEX

Based on detailed measurement of the magnitude and direction of velocity vectors, static pressure, tuft survey on the line of symmetry and paint impression studies on the plan form of the vortex, the basic vortex characteristics like location, rotational velocity, angular velocity, size and strength of the horse shoe vortex have been computed and compared with the data available in the literature. Velocity contours are drawn from the data based on tuft survey, total head diagram, velocity vectors and plan form. The position, size and number of vortices are obtained from the above data. Figures (2.6a to 2.6e) present the various observations made on flow for different vertical positions of the blower.

3.2 Location of the Vortex:

Approximate position of the centre of the vortex could be predicted by the tuft survey. The centre of the vortex has been located from the position of the depression in static pressure curves drawn at wall level and at the level of the vortex centre. This location is checked to be in conformity with velocity and total head vector diagrams and plan form as shown in Figs. (2.6(a) to 2.6 (e)).

The velocity and static pressure distribution at the vortex centre along horizontal and vertical axes are drawn as shown in Figs. (3.1, 3.2). From these figures, it may be observed that the position of the centre of vortex changes alongwith the size of vortex in vertical

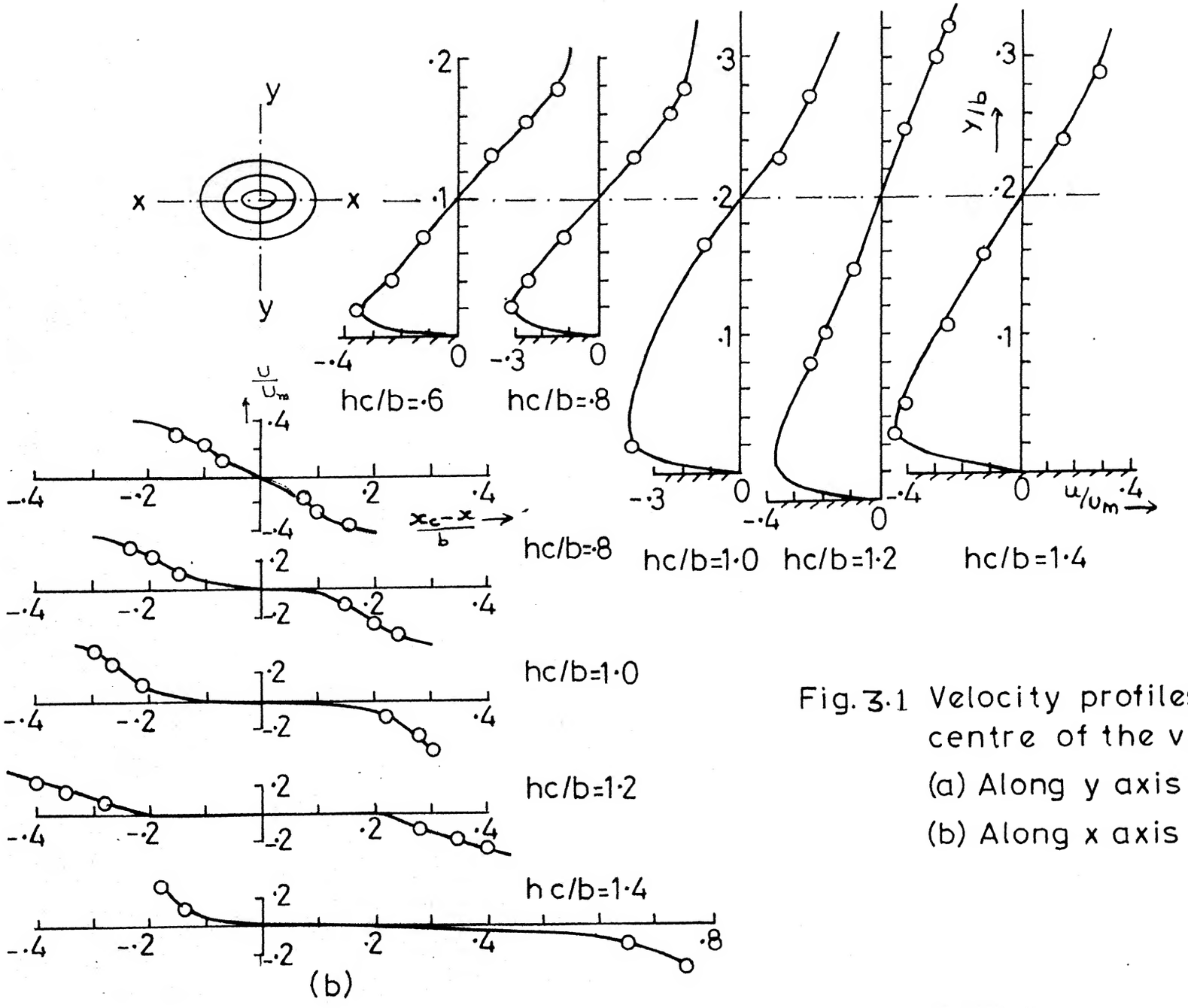

Fig. 3.1 Velocity profiles at the centre of the vortex

(a) Along y axis

(b) Along x axis

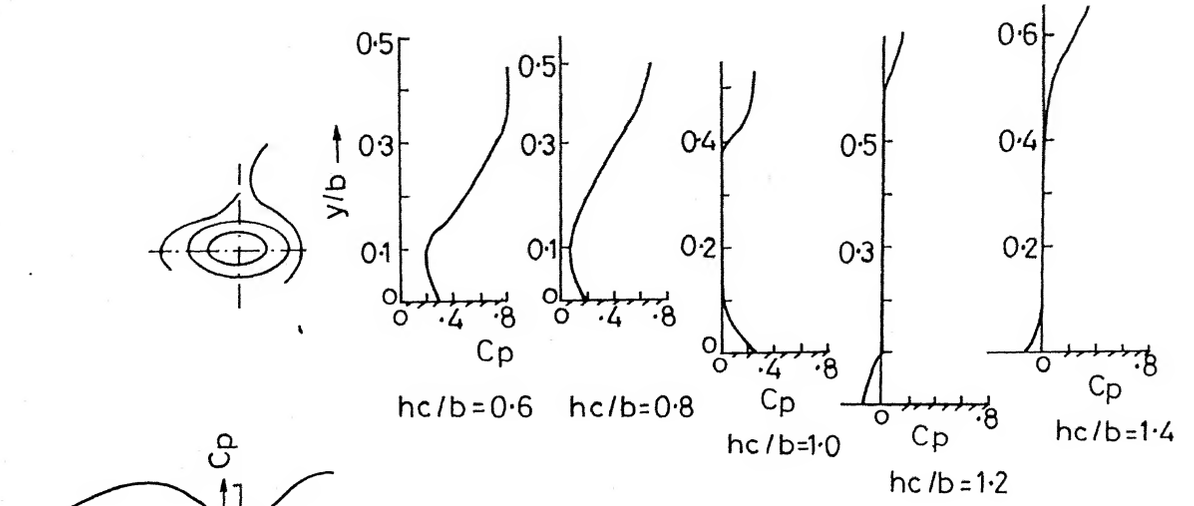

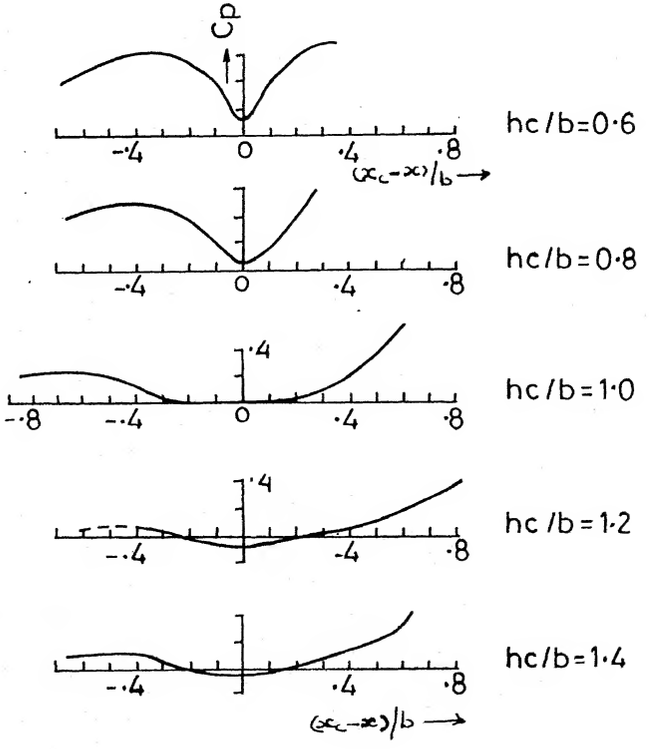

Fig. 3.2 Pressure coefficient profiles at the centre of the vortex
(a) Along y axis
(b) Along x axis

and horizontal directions. The size of the vortex in vertical direction remains fairly same whereas in horizontal direction, it increases indicating the change in shape from circular to elliptical with increase in the height of blower from wall (Fig.3

3.3 Pressure Distribution:

The pressure coefficient at the centre of the vortex designated as c_{pc} and on the wall designated as $c_{p\omega}$ are plotted against the vertical position of the vortex centre as shown in Fig. (3.4a). It may be observed that c_{pc} is lower than c_p for $y_c/b < .14$ and vice versa for $y_c/b > 0.16$ where x_c and y_c are the horizontal and vertical positions of the vortex centre.

The magnitude of pressure depression Δc_p measured from the tangent line to trough in the vertical direction has been obtained separately from the c_p curve on wall as $\Delta c_{p\omega}$ and from c_p curve at the centre of the vortex as Δc_{pc}. The ratio $\Delta c_{pc} / \Delta c_{p\omega}$ is plotted against the position of the vortex centre as shown in Figure (3.4b). It may be observed that the magnitude of the ratio $\Delta c_{pc} / \Delta c_{p\omega}$ decreases with increase in y_c/b and x_c/b (the nondimensionalised vertical and horizontal positions of the vortex centre) and remains fairly independent of the centre position after $y_c/b > .2$, $x_c/b > .5$. The zone of constancy in the ratio $\Delta c_{pc} / \Delta c_{p\omega}$ corresponds to the region where $c_{pc} > c_{p\omega}$ as shown in Fig. (3.4a).

3.4 Strength of the Vortex:

The strength of the horse shoe vortex has been computed from velocity distribution as well as pressure

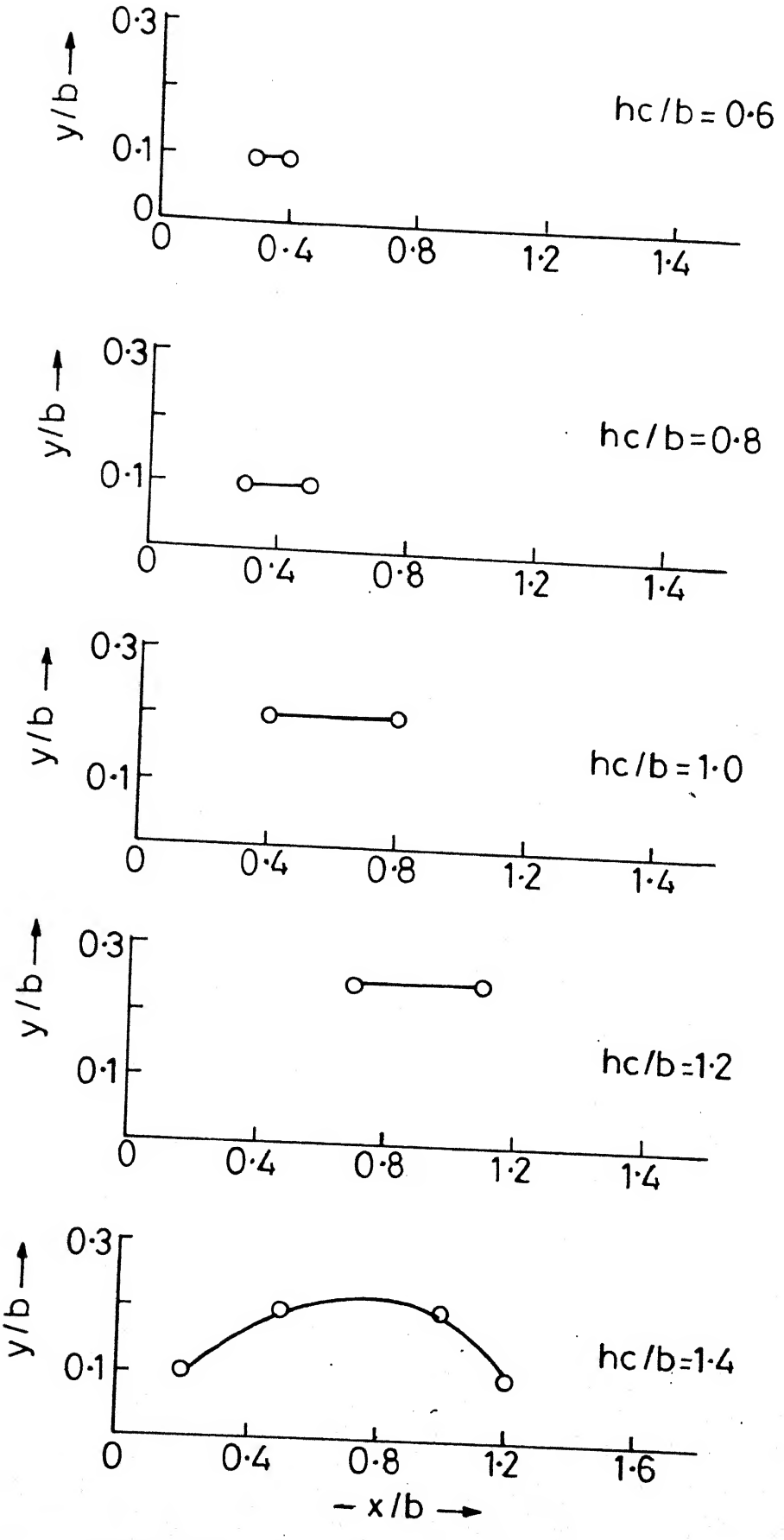

Fig.3·3 Position of the vortex centre

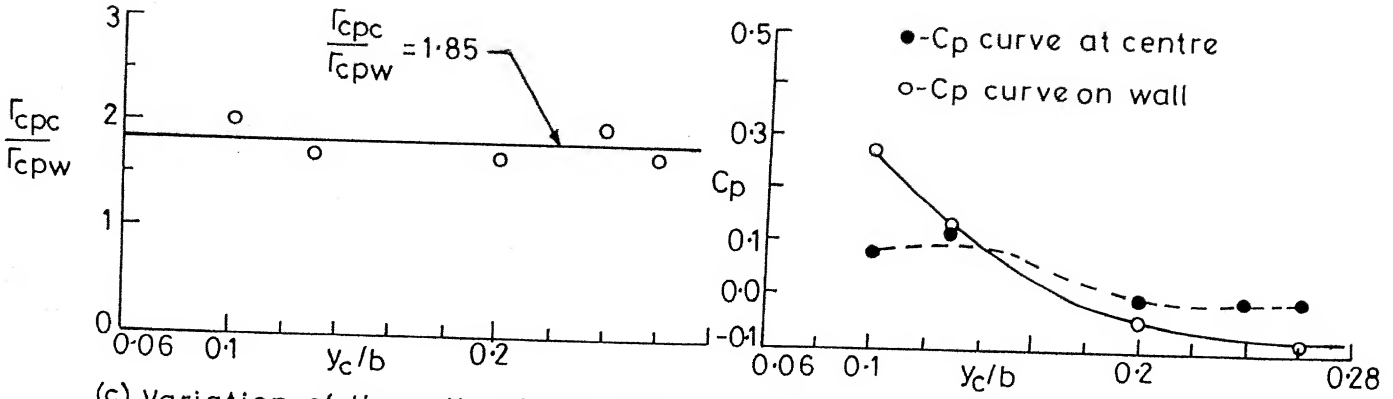

(c) Variation of the ratio of the strengths with the height of the vortex centre

(a) Variation of Cp values at the depression with the height of vortex centre

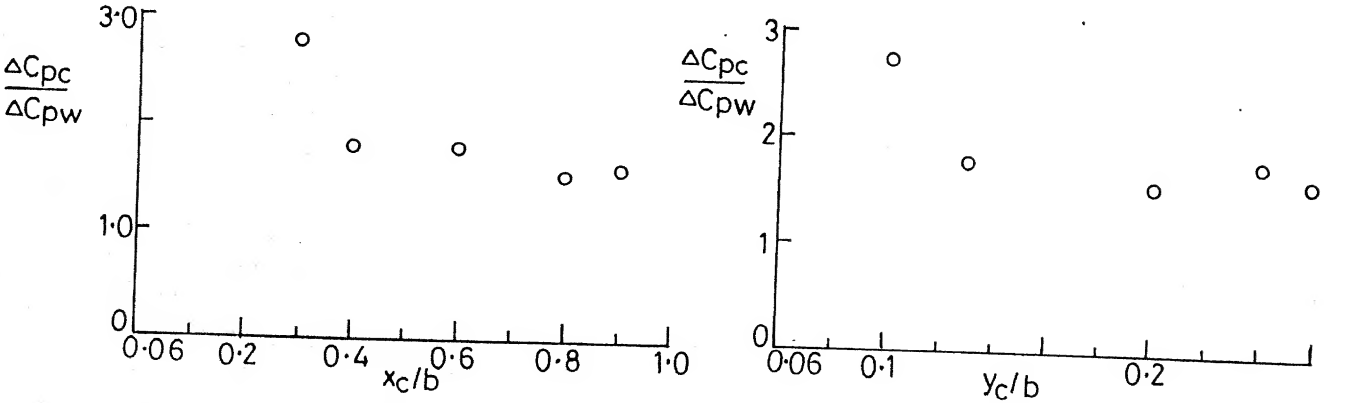

(b) Ratio of the depressions of Cp curves with the position of vortex centre

Fig.3·4 Effect of vortex location on pressure characteristics

distribution on the line of symmetry in the vortex zone.

3.4.1. From Velocity Distribution:

The product of the maximum tangential velocity (V_θ) and corresponding contour perimeter (P_e) gives the strength of the vortex Γ_{V_θ}. The computed values are listed in Table (2.3). Nondimensionalised strength of the vortex $\frac{\Gamma V_\theta}{\pi b U_m}$ was related to the shear Reynolds number $\frac{U_* \delta_*}{\nu}$ as shown in Fig. (3.5). This figure indicates the following relationship for $\frac{\Gamma V_\theta}{\pi b U_m}$ with $\frac{U_* \delta_*}{\nu}$:

$$\frac{\Gamma V_\theta}{\pi b U_m} = .1814 \frac{U_* \delta_*}{\nu} + 9.17 \times 10^{-4} \qquad (3.1)$$

3.4.2. From Pressure Distribution:

Vortices have been identified from the depressions in the pressure distribution curves. Computation of the strength of the vortex has been carried out applying the formula suggested by Gupta (1984). Nondimensionalised strength can be expressed as

$$\frac{\Gamma c_p}{\pi b U_m} = \frac{2r}{b} \sqrt{\Delta c_p} \qquad (3.2)$$

The values of Δc_p and r are measured from c_p curves as indicated in Fig. 1.2.

Vortex strength has been computed from c_p curves on the wall and at the centre of the vortex along the x-axis. Ratio of the two strengths Γc_{pc} and $\Gamma c_{p\omega}$ has been related to the heig of the vortex centre (Fig.3.4(c)). The ratio $\Gamma c_{pc} / \Gamma c_{p\omega}$ appears to be independent of the vertical position of vortex centre y_c and it is found that

$$\frac{\Gamma c_{pc}}{\Gamma c_{p\omega}} = 1.87 \qquad (3.3)$$

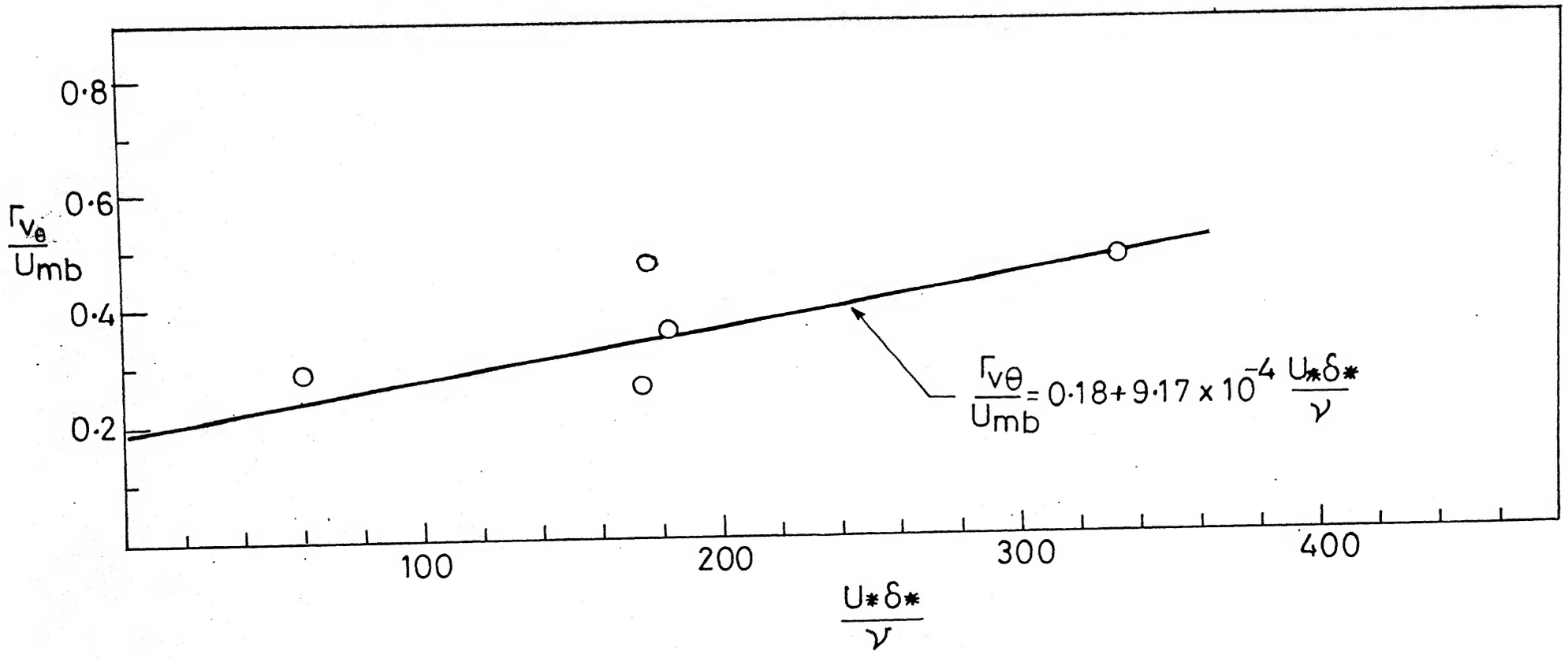

Fig.3·5 Strength of vortex related to undisturbed wall shear Reynolds number based on displacement thickness

3.4.3 Relation between the computed vortex strengths based on the wall pressure distribution and velocity contours:

The computed vortex strength based on the depression in pressure distribution on the wall $\Gamma^*_{c_{p\omega}}$ is related to the strength computed from the velocity distribution $\Gamma^*_{V_\theta}$ (See Fig. 3.6).

An expression may be written as

$$\Gamma^*_{V_\theta} = 0.9 \; \Gamma^*_{c_{p\omega}} \qquad (3.4)$$

3.5 Comparison with Previous Data:

3.5.1 Relation of strength of Horseshoe vortex with Pier Reynolds number

Figure (3.6) shows plot between the nondimensionalised strength computed from the velocity profiles and pressure profiles obtained by various investigators and pier Reynolds number.

Velocity profile at the centre of the vortex obtained by Baker (1979) and Qadar (1981) have been used to compute the strength of the horse shoe vortex assuming that the vortices have circular sections. Strength was given as

$$\frac{\Gamma}{\pi D \bar{U}} \cdot \frac{V_\theta \cdot 2\pi r_o}{\pi D \bar{U}} = \frac{V_\theta}{\bar{U}} \; \frac{2 r_o}{D} \qquad (3.5)$$

where $\frac{V_\theta}{\bar{U}}$ and $\frac{2 r_o}{D}$ have been shown in an illustrative Figure below:

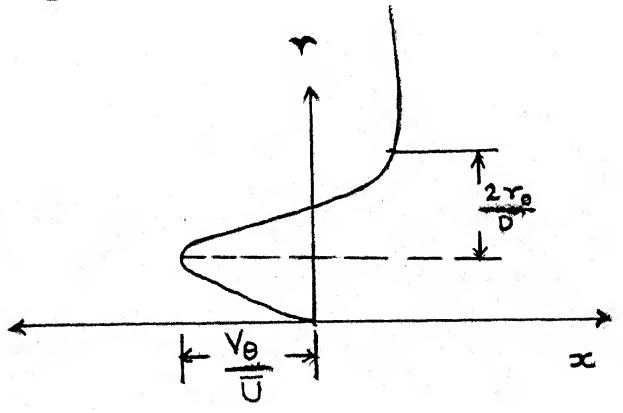

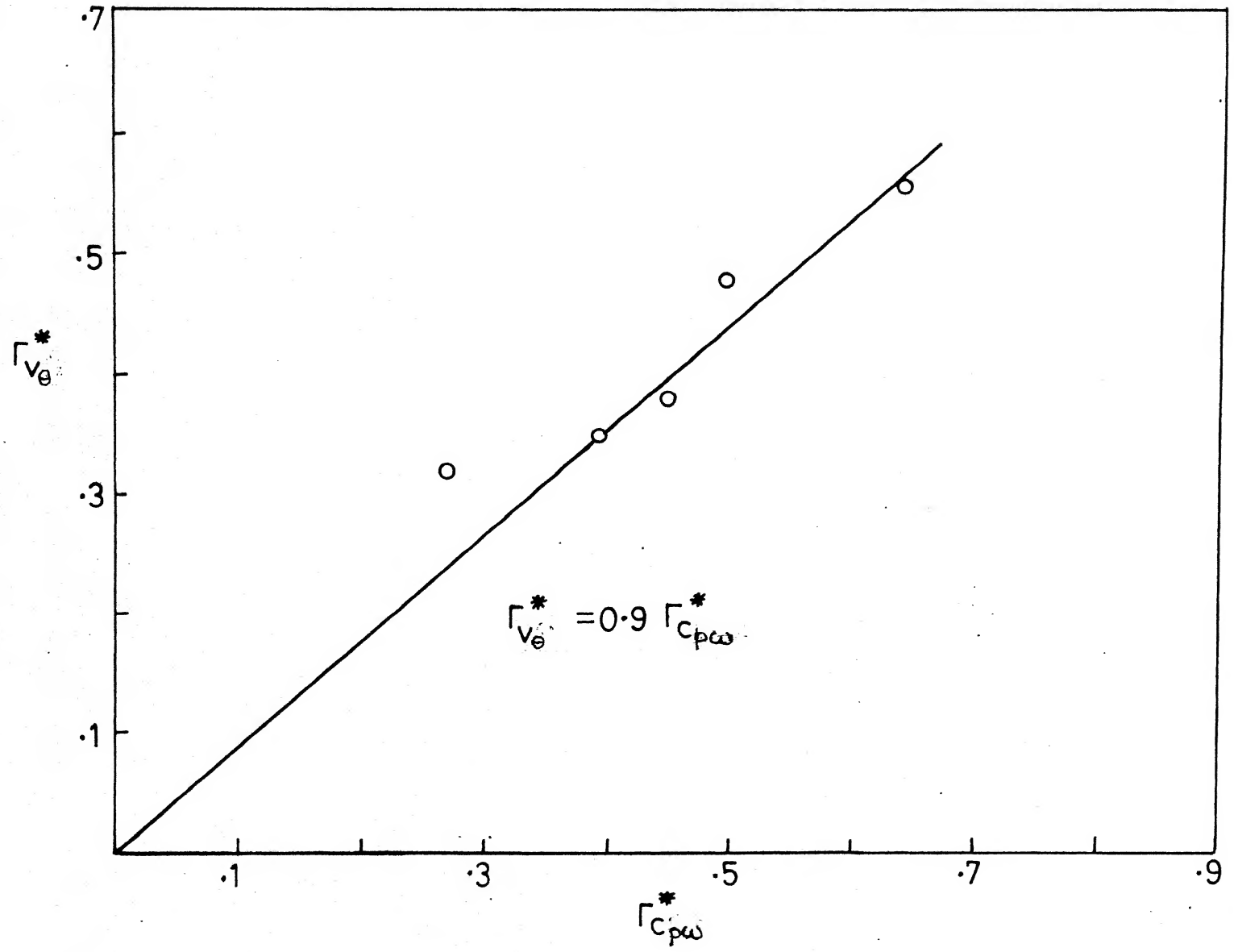

Fig.3·6 Relationship of strength computations based on velocity and pressure distributions

Table 3.1 : Values of strength from circular and elliptical shaped vortex

$\frac{h_c}{b}$	Circular shape $\frac{\Gamma}{\pi b \bar{U}} = \frac{V\theta \cdot 2r_o}{b\bar{U}}$	Actual shape $\frac{\Gamma}{\pi b \bar{U}} = \frac{V\theta \cdot P_e}{\pi b \bar{U}}$	Ratio $\frac{P_e}{2\pi r_o}$
0;6	.060	.097	1.59
0.8	.072	.117	2.21
1.0	.050	.137	2.78
1.2	.061	.193	3.15
1.4	.059	.256	4.35

With the above assumption of the horse shoe vortex as circular with diameter D_o, the corresponding size in the vertical direction has been adopted for the computation of the strength in the present data. These data are plotted in Fig. (3.7) along with the data of other investigators. It may be observed that the present data also agree with other data, and their relationship may be expressed according to Muzzammil, Gupta and Gangadhariah (1986) as

$$\frac{\Gamma}{\pi D \bar{U}} = 90 \, (Re_D)^{-0.7}$$

where $Re_D = \frac{\bar{U} b}{2\nu}$

where Re_D - Reynolds number

In the present investigation, it was observed that the shape of the vortex varied from circular to elliptical. The

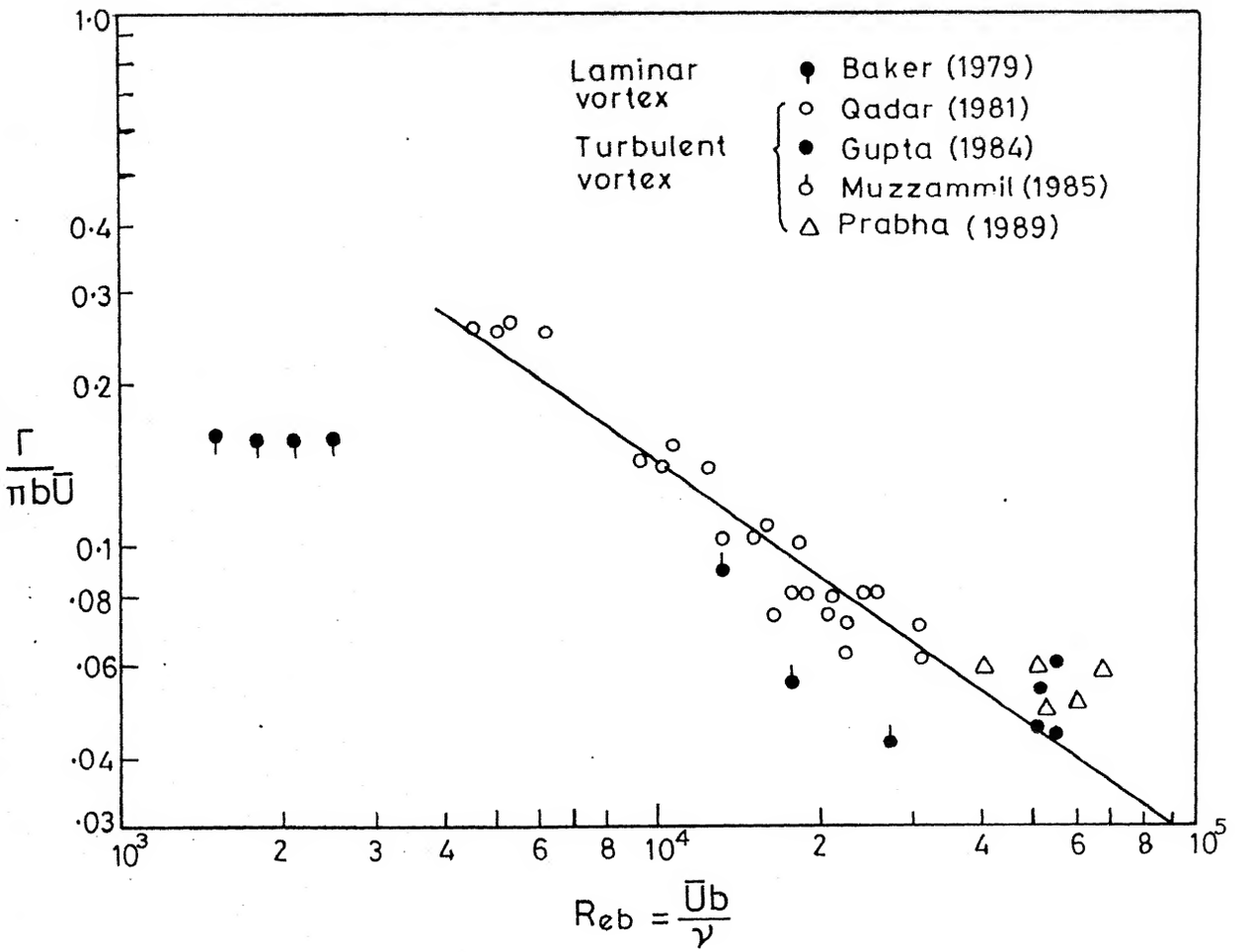

Fig.3.7 Relation between strength of horse shoe vortex with pier Reynolds number

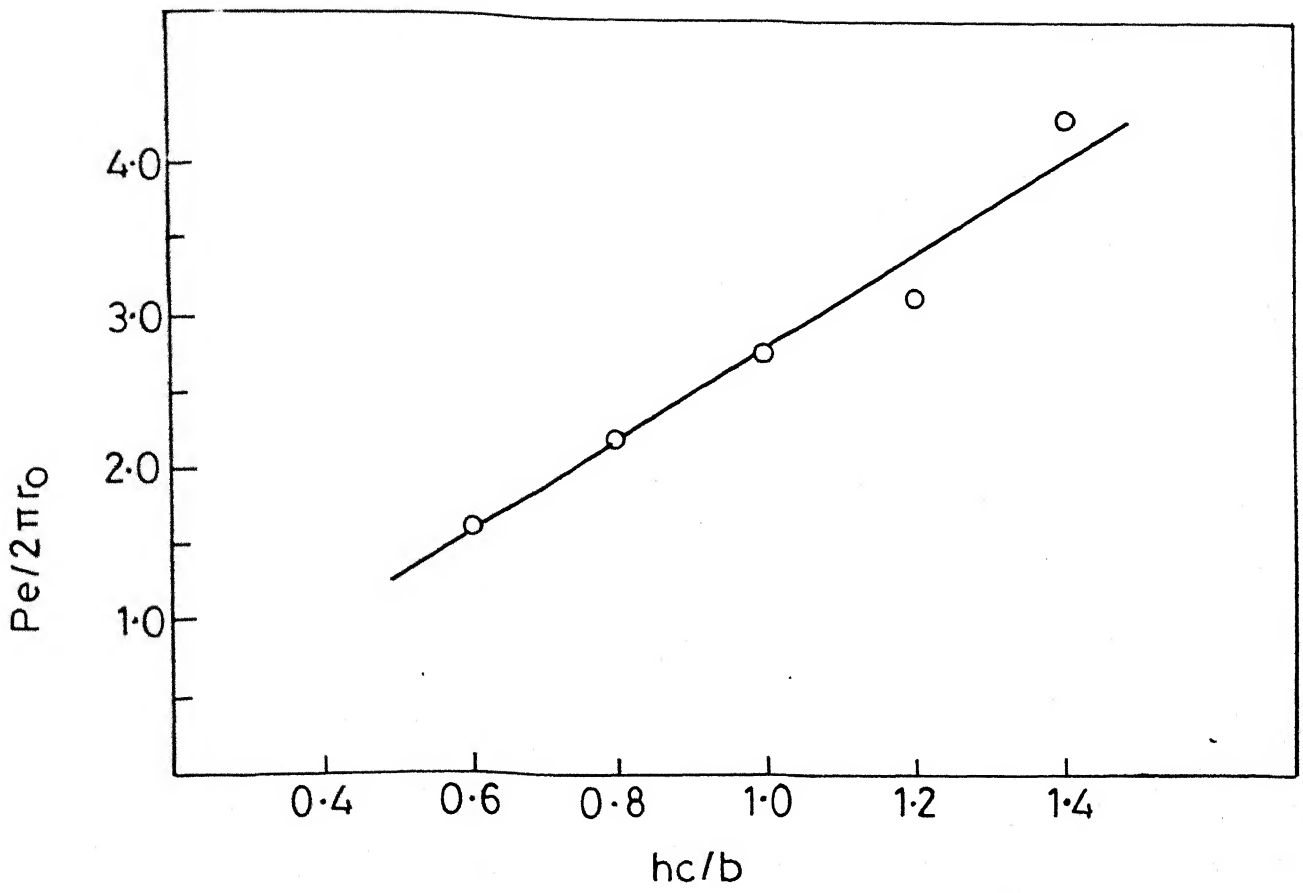

Fig.3·8 Perimeter relationships of horse shoe vortex

computed values of the vortex strength with the assumption of circular shape and that completed with actual shape are listed in Table 3.1.

3.5.2 Relation of rotational velocity V_θ with Pier Reynolds number

The rotational velocity computed from the velocity contours has been nondimensionalised with the average velocity $\bar{U}$ of the undisturbed flow and plotted against the Pier Reynolds number as shown in Fig (3.9).

The magnitude of $\frac{V_\theta}{\bar{U}}$ decreases with increase in pier reynolds number. The present data fall well above the relationship suggested by Muzzammil et al (1989). The expression relating $\frac{V_\theta}{\bar{U}}$ with Re_D is written as

$$\frac{V_\theta}{\bar{U}} = \frac{48}{\sqrt{Re_D}}$$

D is the diameter of the circular cylinder.

3.5.3 Location of the vortex

The Analysis of Baker (1980) suggests that the vortex centre position X_c and separation position X_s are dependent on $\frac{U\delta^*}{\nu}$, Reynolds number based on displacement thickness

The present data are also plotted along with Baker's data as shown in Fig (3.10). The present data points lie well above Baker's data. This is probably due to the shape of the pier. In the present case the pier is rectangular whereas in Baker's data it was circular.

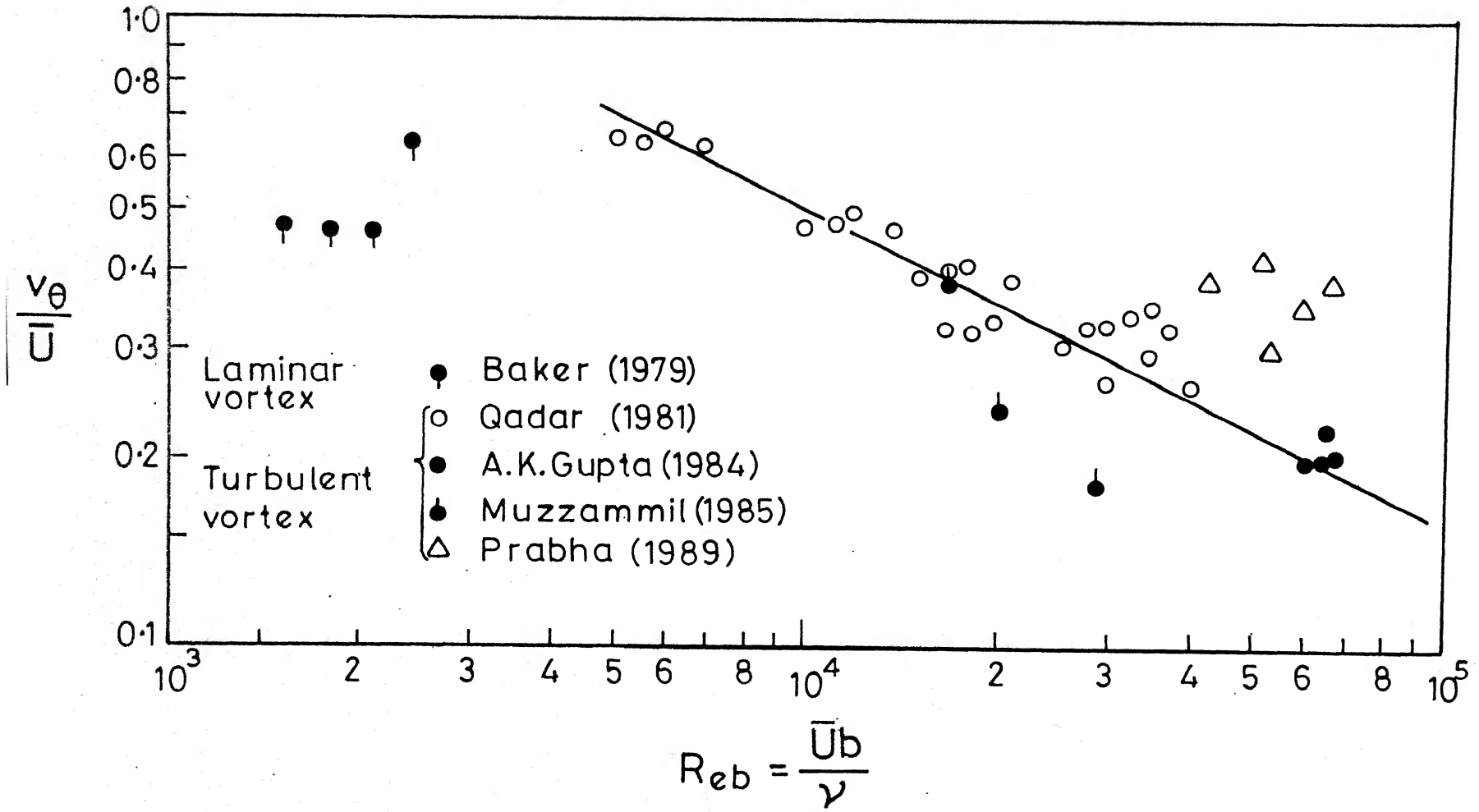

Fig.3·9 Relation between rotational velocity and pier Reynolds number

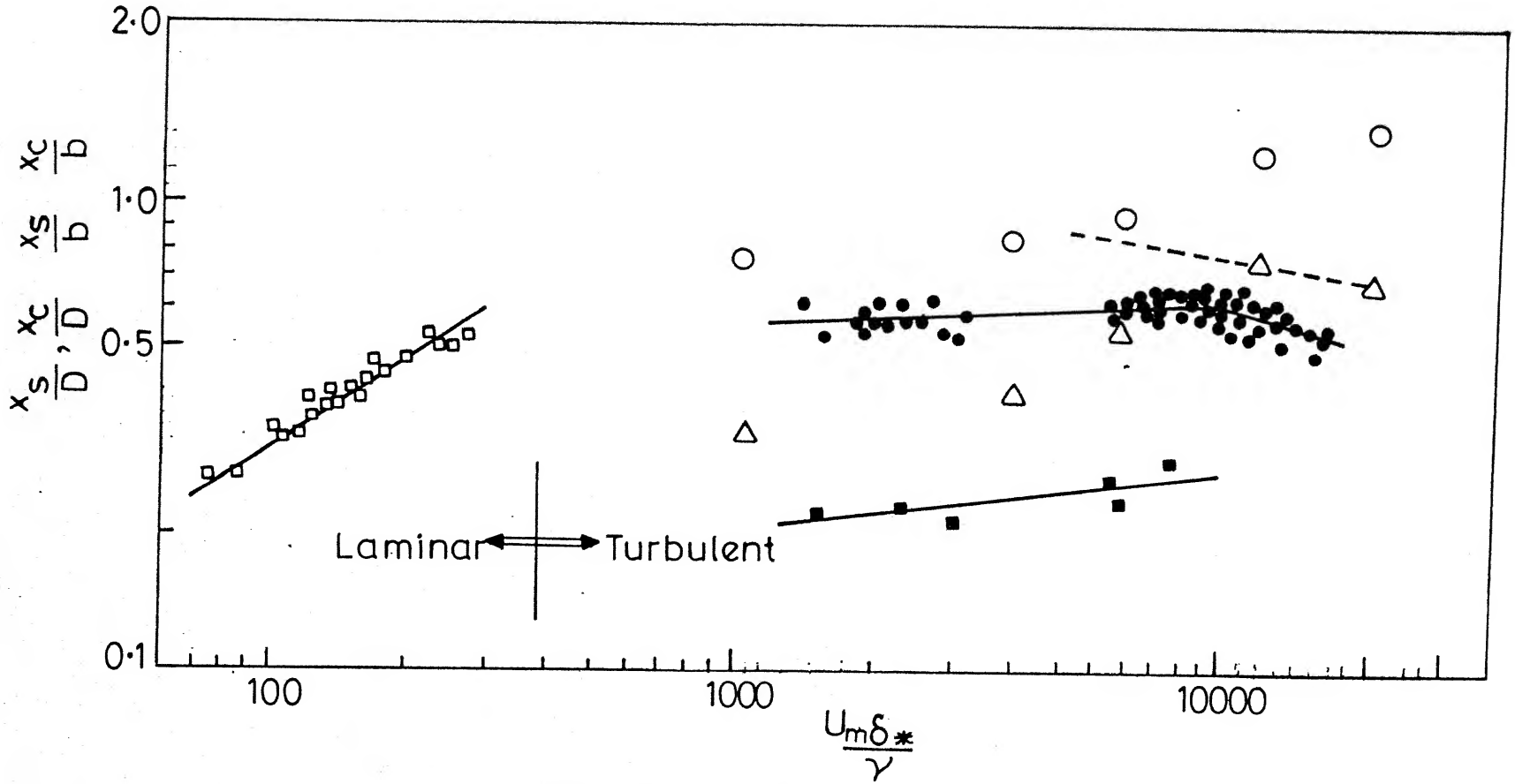

Fig.3·10 Relationship between the position of vortex centre and separation point with $U_m \delta^*/\nu$

3.5.4 Relation of Vorticity with Pier Reynolds number:

The plot of $\frac{\omega b}{\bar{U}}$ with pier reynolds number $\frac{\bar{U}b}{\nu}$ for the data of other investigators is shown in Fig (3.11).

The computation of "ω" with these data was based on the assumption of circular shaped horse shoe vortex. Based on this consideration $\omega = \omega_c$ is computed using size of the vortex in the vertical direction as the diameter of the circular shaped vortex as

$$\frac{\omega_{cb}}{\bar{U}} = \frac{V_\theta}{2\pi r_o} \frac{b}{\bar{U}} \quad \omega_c \text{ in rpm} \qquad (3.6(a))$$

$$\frac{\omega_{cb}}{\bar{U}} = \frac{V_\theta}{2\pi r_o} \cdot \frac{b}{\bar{U}} \times 2\pi \qquad (3.6(b))$$

when ω_c is in radians.

These computed data (shown in table 3.2 are plotted alongwith the data of other investigators as shown in Fig. (3.11). It may be observed that the present are almost twice the corresponding values obtained from the equation -

$$\frac{\omega_o D}{\bar{U}} = 51 \; Re_D^{-0.3} \qquad (3.7)$$

which was suggested by Muzzammil et al (1989).

W_o is initial vorticity of horse show vortex

D is the diameter of circular pier

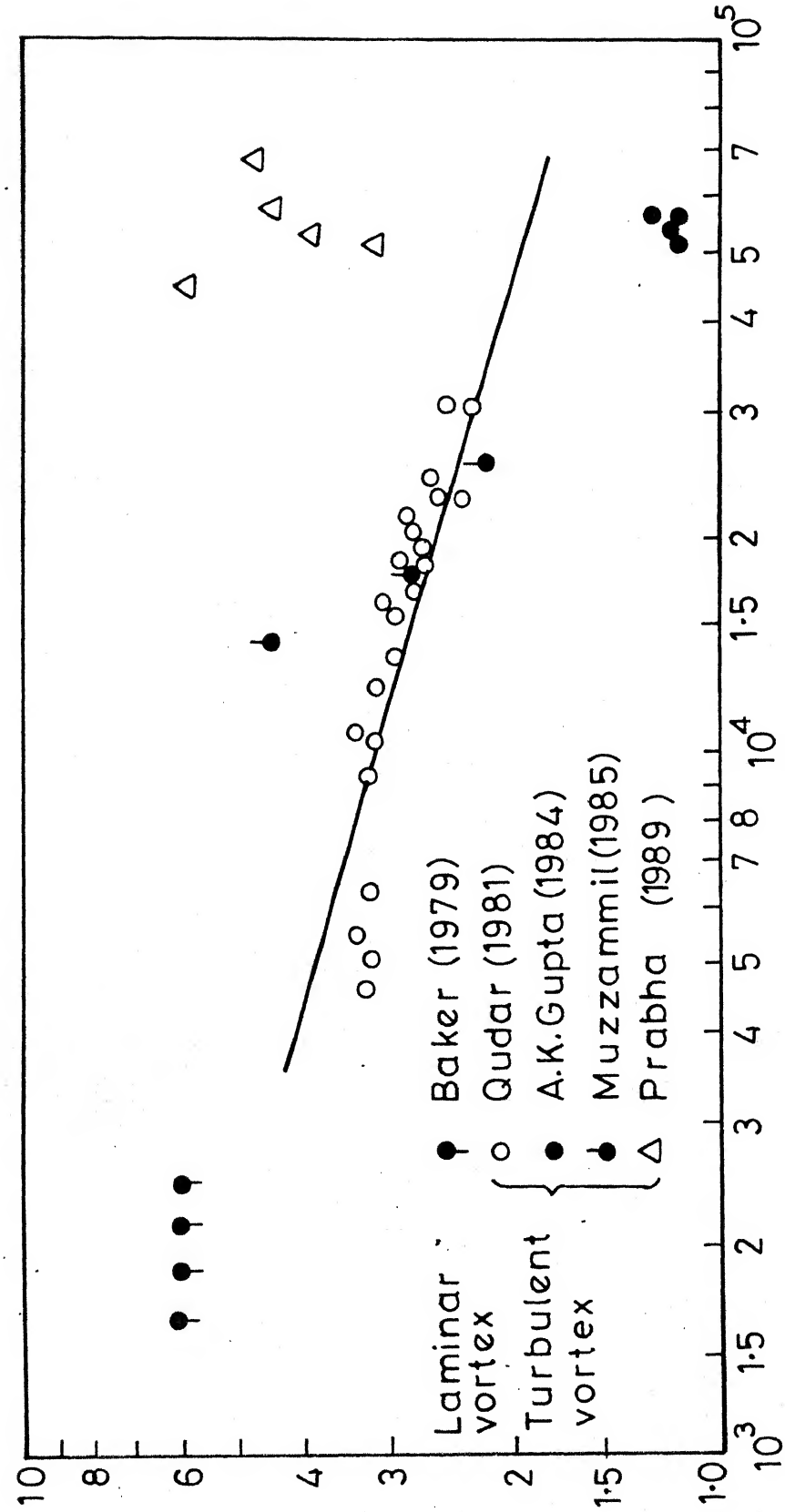

Fig.3.11 Vorticity relation with pier Reynolds number

3.5.5 Relation of Size D_o with Reynolds Number:

Size of horse show vortex D_o, (vertical dimension) measured from the velocity distribution has been nondimensionalised as $\frac{\bar{U}D_o}{\nu}$ and plotted against the pier reynolds number Re_b. Fig (3.12). It may be observed that the present experimental data agrees with the curve proposed by Muzzammil et al.(1989). The relation between size and Reynolds number may be written as

$$\frac{\bar{U}D_o}{\nu} = 1.88\ (Re_D)^{0.8} \qquad (3.8)$$

where D is the diameter of the circular cylinder.

Table 3.2 : Computation of Vorticity

$\frac{h_c}{b}$	$\omega = \frac{V\theta}{P_e}$	$\omega^* = \frac{V\theta}{P_e}\ \frac{b}{U}$	$\frac{P_e}{2\pi r_o}$	$\omega_c^* = (\frac{V\theta}{P_e}\ \frac{b}{U}) \times \frac{P_e}{2\pi r_o}$
0.6	204.00	2.99	1.59	4.76
0.8	130.76	2.15	2.21	4.73
1.0	77.00	1.37	2.78	3.81
1.2	51.28	0.99	3.15	3.15
1.4	55.07	1.2	4.35	5.22

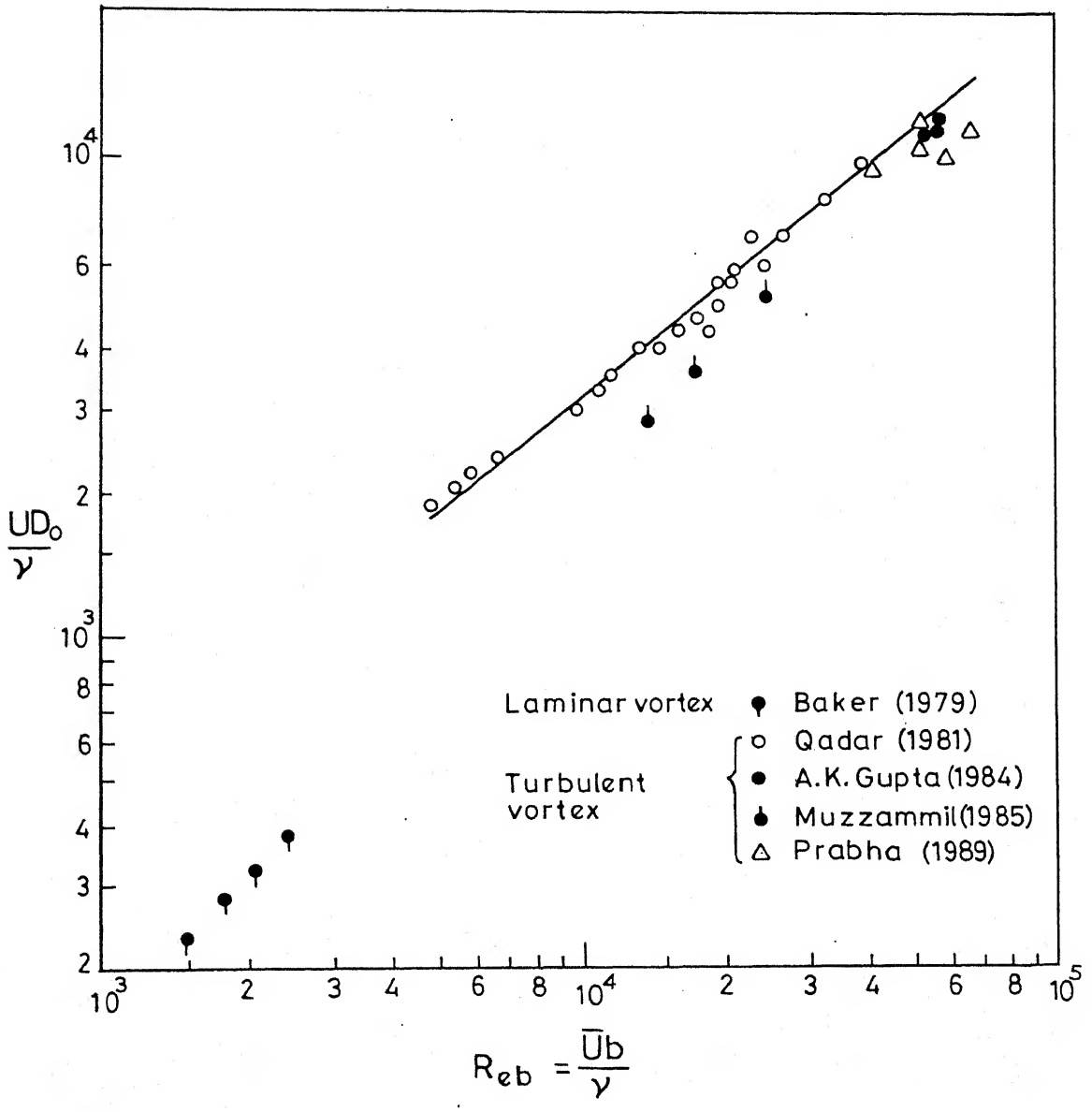

Fig.3·12 Variation of size of horse shoe vortex with pier Reynolds number

3.6 Discussion:

The presence of forced vortex near the junction of cylinder with the wall alter the pressure distribution by causing depression, as observed by Belik, Baker, Gupta and Muzzammil. Gupta developed a method to predict the vortex strength based on depressions in the pressure curves. The depressions obtained on the pressure curves on the wall and at the centre of vortex are not related. This aspect was verified in the present work. It was observed that the ratio of pressure depressions was decreasing as the vortex position raised from the wall up to a certain distance, further raise caused the no change in the magnitude of the ratio.

The strength of horse shoe vortex computed based on pressure depressions was related with strength computed from vertical velocity distribution at centre of vortex by Muzzammil et al. The horse shoe vortex is assumed to be circular in shape in the computation of its strength from velocity distribution. However, it was known that horse shoe vortex was usually elliptical in shape. From the present detailed velocity survey in the vortex zone, it was observed that the shape of the vortex changed from circular to elliptical based on the flow and geometry conditions. The vortex strength based on actual velocity contour has been computed in the present work. It was observed that this vortex strength was much higher than vortex strength computed on the assumption of circular vortex.

The final aim of this investigation was to relate the strength computations based on pressure curve $\Gamma^*_{c_p}$ on the wall with strength computed from velocity contours $\Gamma^*_{v_\theta}$. It was

observed that their relationship was of the order

$$\Gamma^*_{v_\theta} = 0.9 \quad \Gamma^*_{c_{p\omega}}$$

Thus indicating that the curve proposed by Muzzammil et al. (1989) is applicable to predict the strength of horse shoe vortex.

CHAPTER - 4

CONCLUSIONS AND RECOMMENDATIONS

4.1 Conclusions

Experiments were conducted for five positions of blower to measure the pressure and velocity on the line of symmetry in separating zone at the junction of rectangular pier with wall. The vortex strength, size and vorticity were computed from the data obtained. Based on these data, the following conclusions are drawn:

1. Centre of the vortex lies above the data proposed by Baker (See Fig. 3.11).
2. The pressure depression at the vortex centre on the wall and at the horizontal level at centre of vortex was decreasing with increase in the vertical height of vortex centre upto y_c=1.0 cm value and remains fairly constant for further increase in vertical position.
3. The strength computed based on the pressure depressions at the wall were about 0.5 times the strength computed from the pressure depressions at the centre of the vortex.
4. The vortex strength computed from velocity distribution and from the pressure distribution on the wall are nearly of thesame magnitude. This indicates the validity of the curve proposed by Muzzammil et al. (1989) for predicting the horse shoe vortex strength based on pier Reynolds number.
5. The size of the vortex in vertical direction agrees with the data available in literature.

4.2 Recommendations

1. Results of present analysis should be verified using hot wire animometer instead of a keal probe.

2. Detailed velocity and pressure measurements in the horse shoe vortex zone formed when boundary layer flow past a cylindrical pier mounted on wall plate in wind tunnel should be carried out for comparison with the present results.

REFERENCES

1. Baker, C.J. (1979), 'Laminar Horseshoe Vortex', Journal of Fluid Mechanics, Vol. 95, Part 2, pp. 347-367.

2. Baker, C.J. (1980a), 'Theoretical Approach to Prediction of Local Scour Around Bridge Piers', Journal of Hydraulic Research, 1980, Vol. 18, No. 1, pp. 1-12.

3. Baker, C.J. (1980b), 'The Turbulent Horseshoe Vortex', Journal of Wind Engineering and Industrial Aerodynamics, 6, pp. 9-23.

4. Baker, C.J. (1984), 'The Position of Points of Maximum and Minimum Shear Stress Upstream of Cylinders Mounted Normal to Flat Plates', Journal of Wind Engineering and Industrial Aerodynamics, 18 (1985), pp. 263-274.

5. Belik, L. (1973), 'Secondary Flow about Circular Cylinders Mounted Normal to a Flat Plate', Aeronautical Quarterly, Vol. 24, Part I, pp. 47-59.

6. Breusers, M.N.C., G. Nicollet, and H.W. Shen (1977), 'Local Scour Around Cylindrical Piers', Journal of Hydraulic Research, 15, pp. 211-252.

7. Gangadharaiah, T., M. Muzzammil, and K. Subramanya (1986), 'Vortex Strength Approach for Bridge Pier Scour Predictions', Second International Workshop on Alluvial River Problems, University of Roorkee, Roorkee, October 24-26, pp. 151-158.

8. Gupta, A.K. (1984), 'Experimental Investigation: Boundary Layer Flow Past a Circular Cylinder Mounted on a Flat Plate', M.Tech. Thesis, Department of Civil Engineering, Indian Institute of Technology, Kanpur.

9. Gupta, K. (1986), 'Characteristics of Vortex in the Scour Hole', M.Tech. Thesis, Department of Civil Engineering, Indian Institute of Technology, Kanpur.

10. Gupta, A.K. and T. Gangadharaiah (Under publication), 'Local Scour Reduction by a Delta-Wing-Like Passive Device'.

11. Muzzammil, M. (1985), 'Experimental Investigation: Open Channel Flow Past a Circular Cylinder Mounted on a Rigid Bed and on a Mobile Bed', M.Tech. Thesis, Department of Civil Engineering, Indian Institute of Technology, Kanpur.

12. Muzzammil, M., Kailash Gupta, T. Gangadharaiah, and K. Subramanya (1988), 'Vorticity Characteristics of Scouring Horseshoe Vortex', Third International Workshop on Alluvial River Problems, University of Roorkee, Roorkee.

13. Qadar, A. (1981), 'The Vortex Scour Mechanism at Bridge Piers', Proc. Inst. Civil Engrs., Part 2, Vol. 71, pp. 739-757.

14. Shen, H.W., V.R. Schnelder and S. Karaki (1969), 'Local Scour Around Bridge Piers', Proc. ASCE, 95, HY6, pp. 1919-1940.